Exchange and Dzyaloshinskii-Moriya interaction in Rh/Co/Fe/Ir multilayers: Towards skyrmions in exchange-frustrated multilayers

Felix Nickel [1,*] Sebastian Meyer [2] and Stefan Heinze [1,3]

[1]*Institut für Theoretische Physik und Astrophysik, Christian-Albrechts-Universität zu Kiel, D-24098 Kiel, Germany*

[2]*Nanomat/Q-mat/CESAM, Université de Liège, B-4000 Sart Tilman, Belgium*

[3]*Kiel Nano, Surface, and Interface Science (KiNSIS), University of Kiel, D-24098 Kiel, Germany*

(Received 3 February 2023; accepted 15 May 2023; published 30 May 2023)

We study the magnetic interactions in transition-metal multilayers composed of Co layers and Co/Fe bilayers sandwiched between Ir and Rh layers based on density functional theory (DFT). By mapping our total energy DFT calculations of collinear and noncollinear spin states including spin-orbit coupling to an atomistic spin model we extract the intra- and interlayer exchange constants, the intra- and interlayer Dzyaloshinskii-Moriya interaction constants and the magnetocrystalline anisotropy energies of several multilayers. We demonstrate that the exchange frustration, which stabilizes zero-field sub-10 nm magnetic skyrmions in Rh/Co films on the Ir(111) surface [S. Meyer *et al.*, Nat. Commun. **10**, 3823 (2019)], can be transferred to multilayers formed by a repetition of Rh/Co/Ir trilayers. Increasing the number of Co layers reduces the exchange frustration whereas with adding Fe, a sufficient exchange frustration and strength of the Dzyaloshinskii-Moriya interaction can be obtained to stabilize topological spin structures such as skyrmions in Rh/Co/Fe/Ir multilayers. We show that the exchange interaction in Rh/Co/Fe/Ir multilayers results from the interplay of strong frustration of intralayer exchange in the Fe layer, weak ferromagnetic intralayer exchange in the Co layer, and ferromagnetic interlayer Fe-Co exchange. We analyze the Dzyaloshinskii-Moriya interaction in terms of inter- and intralayer contributions as well as its sign based on the electronic structure of Co/Fe based multilayers with different stacking sequences.

DOI: 10.1103/PhysRevB.107.174430

I. INTRODUCTION

Magnetic skyrmions [1]—localized, stable spin structures—possess intriguing topological and dynamical properties [2], which make them ideally suited for a number of future applications [3,4] ranging from magnetic data storage [5] to neuromorphic computing [6]. In order to realize this potential it is essential to find material systems hosting skyrmions with the desired properties such as nanoscale size, long lifetime, and stability in zero magnetic field [3]. In ultrathin films at surfaces stable magnetic skyrmions with diameters below 10 nm have been observed at low temperatures [7,8] and even without an applied external magnetic field [9].

For applications magnetic multilayers are extremely promising since they are well established in the field of spintronics and allow tuning of the magnetic interactions and thereby skyrmion properties by interfaces between different magnetic and nonmagnetic layers, the chemical composition, and structure [10–15]. With this approach magnetic skyrmions at room temperature have been realized, which can be efficiently moved by electrical currents [11,16–20]. However, the smallest skyrmions, which have so far been obtained still possess diameters above 20 nm. Therefore, the quest of realizing sub-10 nm skyrmions in multilayers is still ongoing. In addition, it is desirable for applications to obtain different coexisting topological spin structures, e.g., skyrmions and antiskyrmions in one material as recently observed with diameters of about 150 nm [21–23]. It has further been shown that systems with frustrated exchange interactions are suited for coexisting sub-10 nm skyrmions and antiskyrmions [24–26]. A competition between exchange frustration and DMI contribution plays also an important role for the formation of isolated spin structures in two-dimensional van der Waals magnets [27–30].

Here, we demonstrate by means of first-principles calculations based on density functional theory (DFT) how the magnetic properties of an ultrathin film system hosting nanoscale skyrmions can be transferred to transition-metal multilayer systems. We consider the film system of an atomic Rh/Co bilayer on the Ir(111) surface [Fig. 1(a)] as a starting point of our study since zero-field sub-10 nm magnetic skyrmions have been experimentally observed [9]. It has been shown via DFT calculations and atomistic spin simulations that skyrmions are stabilized in this system [9] due to the interplay of strong exchange frustration and Dzyaloshinskii-Moriya interaction (DMI). We consider multilayers composed of hexagonal atomic Co, Rh, and Ir layers with the in-plane lattice constant of the Ir(111) surface. Our DFT calculations show that multilayers composed of Rh/Co/Ir trilayers [Fig. 1(b)] exhibit nearly identical magnetic interactions as the film system Rh/Co/Ir(111) implying the existence of zero-field nanoscale skyrmions. Multilayers built from Rh/Co/Rh trilayers possess a similarly strong exchange frustration but

*nickel@physik.uni-kiel.de

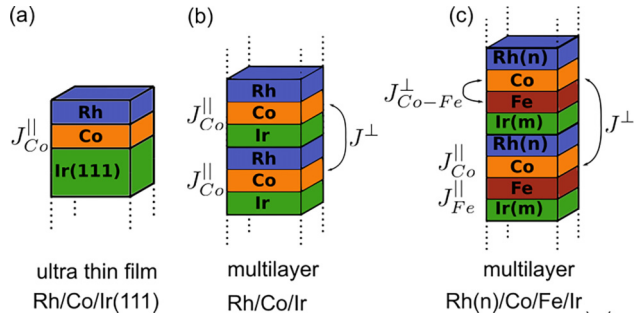

FIG. 1. (a) Sketches of the ultrathin film system Rh/Co/Ir(111) and of the multilayer systems (b) Rh/Co/Ir and (c) Rh(n)/Co/Fe/Ir(m), where n and m denote the number of atomic Rh and Ir layers. Note that the multilayers [(b),(c)] are formed by an infinite repetition of the basic layer structure in the direction perpendicular to the layers. For each of the systems two unit cells are shown. The intra- and interlayer exchange interactions are marked at the corresponding layers. In (c) one can see all possible interactions, which are intralayer interactions within the same atomic layer ($J^{\parallel}_{\mathrm{Fe}}$ and $J^{\parallel}_{\mathrm{Co}}$), interlayer interactions within the same magnetic bilayer ($J^{\perp}_{\mathrm{Co-Fe}}$) and interlayer interactions between bilayers ($J^{\perp}$).

display vanishing DMI due to their inversion symmetric structure.

For potential applications it is necessary to increase the thickness of the magnetic material. Therefore, we studied Co bilayers sandwiched between Rh and Ir. However, in these multilayers the exchange frustration decreases significantly and the DMI is too weak, which prohibits skyrmion formation. We show that a solution to this difficulty is the usage of Co/Fe bilayers sandwiched between Rh and Ir [Fig. 1(c)]. Our DFT calculations demonstrate that the favorable magnetic properties of the Rh/Co/Ir(111) film, i.e., strong exchange frustration and significant DMI, can be transferred to multilayers built from a repetition of Rh/Co/Fe/Ir sandwiches. A decomposition of the exchange interactions into inter- and intralayer contributions shows that Fe/Ir interfaces lead to strong exchange frustration in Fe, while the intralayer exchange in Co is ferromagnetic. Fe and Co layers couple ferromagnetically such that the interaction at the Fe/Ir interface becomes the driving force of the exchange frustration in the multilayer. For Rh/Co/Fe/Ir multilayers, the DMI is even larger than for the ultrathin film system Rh/Co/Ir(111) due to its Fe/Ir interface, while a small DMI favoring spin structures with an opposite rotational sense results in Rh/Fe/Co/Ir multilayers due to the competition of contributions from the Rh/Fe and Co/Ir interface.

This paper is structured as follows. In Sec. II the atomistic spin model of the multilayers is presented and how the interaction constants are obtained based on total energy DFT calculations. The computational details of our DFT calculations are given in Sec. III. The results are presented in Sec. IV. We start with the properties of Rh/Co/Ir multilayers consisting of only one Co layer and compare them to the film system Rh/Co/Ir(111). Then we turn to multilayers formed by a repetition of sandwich structures possessing a magnetic Co bilayer or a Co/Fe bilayer. We analyze the calculated shell-resolved intra- and interlayer exchange interactions, the effective intra- and interlayer DMI, as well as the magnetocrystalline anisotropy of these multilayers. Finally, we discuss the magnetic ground state of the most promising multilayer systems. In the Appendix the results of a number of additional DFT calculations for multilayers with varied stacking orders and compositions including Rh/Co/Rh based multilayers are presented.

II. COMPUTATIONAL METHOD AND SPIN MODEL

To obtain insight into the magnetic interactions of multilayer systems we have performed DFT total energy calculations of collinear and noncollinear spin structures including spin-orbit coupling and mapped these onto an atomistic spin model. The Hamiltonian of the spin model contains the exchange interaction, the DMI, and the magnetocrystalline anisotropy energy (MAE), and is given by

$$H = -\sum_{i,j} J_{ij}(\mathbf{m}_i \cdot \mathbf{m}_j) - \sum_{i,j} \mathbf{D}_{ij}(\mathbf{m}_i \times \mathbf{m}_j) + \sum_i K\left(m_i^z\right)^2 \tag{1}$$

where J_{ij} is the exchange constant between normalized magnetic moments $\mathbf{m}_i$ and $\mathbf{m}_j$ and i and j index two atoms at lattice sites $\mathbf{R}_i$ and $\mathbf{R}_j$. $\mathbf{D}_{ij}$ are the DMI vectors, which denote the coupling strength and direction of the DMI and K is the contribution of the magnetocrystalline anisotropy energy for a system with uniaxial anisotropy.

As shown in Fig. 1(a), in an ultrathin film system such as Rh/Co/Ir(111) only interactions within the magnetic layer can occur denoted as intralayer interactions. In a multilayer built, for example, from an infinite repetition of the three layers Rh/Co/Ir [Fig. 1(b)], additional interlayer interactions acting between two magnetic layers are possible. For systems with more than one atomic layer per magnetic layer [Fig. 1(c)], there are further interactions within the magnetic layer as illustrated for a multilayer built from the repetition of a Rh/Co/Fe/Ir sandwich structure.

Within our DFT based approach, we use the energy dispersions of flat spin spirals calculated without spin-orbit coupling (SOC) to determine the exchange interaction. For every calculated spin spiral state, we add SOC in first-order perturbation theory and get access to the DMI. The third term in Eq. (1) is determined self-consistently in separate collinear calculations including SOC where we apply the spin-quantization axes along different lattice directions. For the first two terms in Eq. (1), we determine both inter- and intralayer contributions, while for the MAE, we restrict ourselves to the total contribution of the system.

In the following we present how the magnetic interactions in these systems can be categorised and determined in detail.

A. Energy dispersion of flat spin spirals

The DFT total energies of different collinear and noncollinear spin structures are calculated using the full-potential linearized augmented plane-wave (FLAPW) method as implemented in the FLEUR code [31–33]. To scan a large part of the magnetic phase space spin spirals are considered. A spin spiral state is characterized by a wave vector $\mathbf{q}$ from the Brillouin zone and the magnetic moment of an atom at lattice site $\mathbf{R}_i$ is given by $\mathbf{M}_i = M(\cos(\mathbf{q}\cdot\mathbf{R}_i), \sin(\mathbf{q}\cdot\mathbf{R}_i), 0)$, where M is

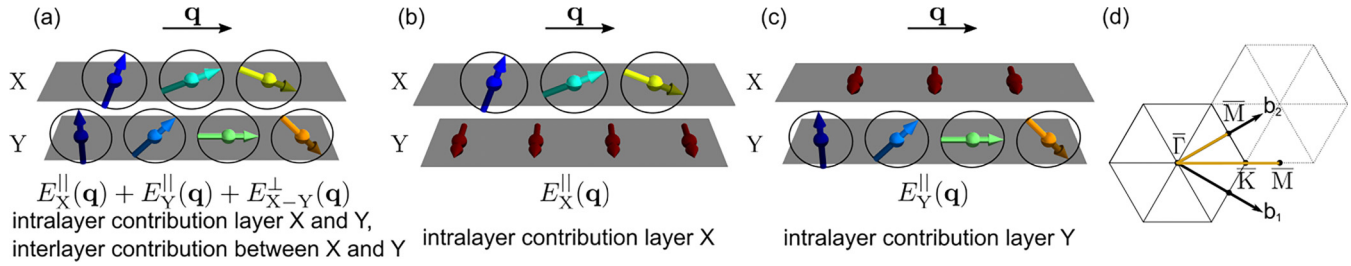

FIG. 2. Sketches of flat cycloidal spin spirals propagating in a magnetic bilayer along the direction of the wave vector $\mathbf{q}$. The energy contributions of each spin spiral are given below the sketches. (a) The spin spiral propagates in both the X and the Y layer. (b) The spin spiral propagates only in the top (X) layer, while all spins in the bottom (Y) layer are parallel with respect to each other and oriented perpendicular to the rotation plane of the spin spiral in the top layer. (c) The spin spiral propagates only in the bottom (Y) layer, while all spins in the top (X) layer are parallel with respect to each other and oriented perpendicular to the rotation plane of the spin spiral in the bottom layer. (d) Sketch of the hexagonal two-dimensional Brillouin zone and the high symmetry directions along which $\mathbf{q}$ is chosen for the spin spirals.

the magnitude of the magnetic moment. If SOC is neglected all magnetic lattice sites are equivalent and the generalized Bloch theorem [34,35] can be applied. This allows to use the chemical unit cell rather than the magnetic unit cell for the calculation of the energy dispersion $E(\mathbf{q})$ of spin spirals. The SOC contribution to the energy dispersion of spin spirals can be calculated in first-order perturbation theory [33]. From these energy contributions due to SOC the DMI can be determined [36].

For a system consisting of two magnetic layers, denoted as X and Y, a spin spiral defined by $\mathbf{q}$ can be propagating in both layers as shown in Fig. 2(a). The pairwise interactions in those two layers and the corresponding interaction energies $E(\mathbf{q})$ can be categorized into three groups. First, there are interactions between two lattice sites from the layer X with the corresponding energy $E^{\parallel}_{X}(\mathbf{q})$, this is the intralayer exchange of layer X. Analogously, there are interactions between two lattice sites in layer Y with energy $E^{\parallel}_{Y}(\mathbf{q})$—the intralayer exchange of layer Y. The third group consists of interactions, in which one lattice site is located in layer X and the other one in layer Y. The energy representing those interactions denoted as $E^{\perp}_{X-Y}(\mathbf{q})$ is the interlayer exchange between layer X and Y. The total energy of this magnetic bilayer system with layers X and Y is given by

$$E(\mathbf{q}) = E^{\parallel}_{X}(\mathbf{q}) + E^{\parallel}_{Y}(\mathbf{q}) + E^{\perp}_{X-Y}(\mathbf{q}) \quad . \tag{2}$$

This method of categorising pairwise interactions can be extended in the same manner for more layers (cf. Fig. 2).

Besides a spin spiral propagating in all layers [Fig. 2(a)], it is possible to set up a spin spiral propagation only in one of the layers. This setup is shown in Figs. 2(b) and 2(c). For specific setups some contributions on the right-hand side of Eq. (2) vanish. To determine the three contributions of the right-hand side of Eq. (2) individually we use different setups, which are described in detail in the following.

1. Intralayer contributions

To obtain the energies $E^{\parallel}_{X}(\mathbf{q})$ we use spin spirals with varying $\mathbf{q}$ propagating in layer X [cf. Fig. 2(b)]. In this way, only the intralayer interactions $E^{\parallel}_{X}(\mathbf{q})$ contribute to the energy $E(\mathbf{q})$. This is illustrated in Fig. 2(b), where the top layer represents the layer X. In addition, one has to make sure that the other layer Y does not contribute to the energy. Therefore, all spins in the other layer are fixed in the ferromagnetic state as shown in Fig. 2(b). Thereby, the spins in layer Y do not vary with $\mathbf{q}$ and only contribute a constant energy $E_Y(\mathbf{q}=0) = E^{\mathrm{FM}}_{Y}$ to $E(\mathbf{q})$. This constant contribution vanishes, when comparing all energies to the FM state. To ensure that the interlayer contributions $E^{\perp}_{X-Y}(\mathbf{q})$ also vanish, the spins in layer Y need to be perpendicular to all spins from layer X [Fig. 2(b)].

For the exchange interaction one can see directly that the contribution for a magnetic moment $\mathbf{m}^X_i$ in layer X and $\mathbf{m}^Y_j$ in layer Y vanishes as $\mathbf{m}^X_i \cdot \mathbf{m}^Y_j = 0$ if $\mathbf{m}^X_i \perp \mathbf{m}^Y_j$ [compare Eq. (1)]. By taking only the in-plane component of the DMI vector $\mathbf{D}_{ij}$ into account the term $\mathbf{D}_{ij}(\mathbf{m}^X_i \times \mathbf{m}^Y_j)$ from Eq. (1) vanishes. This approximation is further discussed later. This vanishing term leads to a vanishing interlayer DMI contribution for the described spin structure. With this spin structure it is now possible to determine $E^{\parallel}_{X}(\mathbf{q})$. $E^{\parallel}_{Y}(\mathbf{q})$ can be calculated in the same way. But now the spin spiral has to propagate in the Y layer and all spins of the X layer have to be fixed and perpendicular to all spins of the Y layer. This is illustrated in Fig. 2(c).

2. Interlayer contributions

If a spin spiral propagates in both magnetic layers X and Y [Fig. 2(a)] both intralayer interaction terms, i.e., $E^{\parallel}_{X}(\mathbf{q})$ and $E^{\parallel}_{Y}(\mathbf{q})$, contribute to the energy dispersion $E(\mathbf{q})$. Additionally, the interlayer interactions $E^{\perp}_{X-Y}(\mathbf{q})$ contribute since in general $\mathbf{m}^X_i$ is not perpendicular to $\mathbf{m}^Y_j$. Hence all three interactions are present [cf. Eq. (2)]. However, $E^{\parallel}_{X}(\mathbf{q})$ and $E^{\parallel}_{Y}(\mathbf{q})$ are already known from the previous calculations [cf. Figs. 2(b) and 2(c)]. Therefore, one can obtain $E^{\perp}_{X-Y}(\mathbf{q})$ by subtracting the contributions of each layer from the total dispersion $E(\mathbf{q})$ for a spin spiral propagating in both layers. When these calculations fulfill these conditions in principle any $\mathbf{q}$ can be used. As long as no atoms in layer X have the same x and y coordinate as any atom in the layer Y one can restrict $\mathbf{q}$ to lie within the xy plane. This restriction allows to directly compare the spin spiral energy dispersions to those of monolayer systems and still makes is possible to calculate all interactions. This is used for all interactions discussed in the main text. The case for layers where atoms share the same x and y coordinates is described in Appendix D.

B. Magnetic interactions

1. Exchange interactions

To obtain the exchange interaction constants within a single magnetic mono- or bilayer, i.e., for the example of Fig. 1(c) $J^{||}_{\mathrm{Co}}$, $J^{||}_{\mathrm{Fe}}$, and $J^{\perp}_{\mathrm{Co-Fe}}$, spin spirals characterized by $\mathbf{q}$ along the high-symmetry directions $\overline{\mathrm{M}}-\overline{\Gamma}-\overline{\mathrm{K}}-\overline{\mathrm{M}}$ of the two-dimensional (2D) hexagonal Brillouin zone (BZ) were used [see Fig. 2(d)]. As described above the energy contributions are categorised in two intralayer contributions for the layers X and Y and an interlayer contribution. For each of those interactions the first term of Eq. (1) can be evaluated. Without loss of generality $\mathbf{m}_i$ is assumed to point in a constant direction and $\mathbf{m}_j = \mathbf{m}_j(\mathbf{q})$ is a function of $\mathbf{q}$. The magnetic moments $\mathbf{m}_j(\mathbf{q})$ are sorted in shells under the condition that the distance $|\mathbf{R}_j - \mathbf{R}_i|$ is the same for every j in the same shell. The interactions between each magnetic moment $\mathbf{m}_j(\mathbf{q})$ of the same shell n and the reference moment $\mathbf{m}_i$ are equal due to the symmetry of the system. All exchange interactions within a bilayer have now the form

$$E_{\mathrm{ex}}(\mathbf{q}) = -\sum_n J_X^{||,n} \sum_j \cos(\mathbf{q}\mathbf{R}_j) - \sum_n J_Y^{||,n} \sum_j \cos(\mathbf{q}\mathbf{R}_j) - \sum_n J_{X-Y}^{\perp,n} \sum_j \cos(\mathbf{q}\mathbf{R}_j). \tag{3}$$

In the first sum n is the shell index and in the second sum j denotes the different sites within shell n. $J_X^{||,n}$, $J_Y^{||,n}$, and $J_{X-Y}^{\perp,n}$ are the shell-resolved intra- and interlayer exchange constants, respectively.

2. Dzyaloshinskii-Moriya interaction

When SOC is taken into account, DMI and MAE contribute to the total energy of a given spin configuration. In particular, clockwise and counterclockwise rotating cycloidal spin spirals are not energetically degenerate and the generalized Bloch theorem cannot be used anymore. This makes the self-consistent calculation of the energy of spin spirals with SOC, e.g., by using super cells, computationally very time consuming. Because the DMI is typically much smaller than the exchange interaction, it is treated as a perturbation. The self-consistently determined Kohn-Sham states of a spin spiral without SOC $|\Psi_{\mathbf{k},\nu}(\mathbf{q})\rangle$ are used to calculate the energy due to SOC $\delta\epsilon_{\mathbf{k},\nu}(\mathbf{q})$ in first-order perturbation theory using the SOC operator H_{SOC} [33,37],

$$\delta\epsilon_{\mathbf{k},\nu}(\mathbf{q}) = \langle\Psi_{\mathbf{k},\nu}(\mathbf{q})|H_{\mathrm{SOC}}|\Psi_{\mathbf{k},\nu}(\mathbf{q})\rangle. \tag{4}$$

Integration over the 2D-BZ and summation over all bands ν gives the total energy contribution for spin spirals due to SOC denoted as $\Delta E_{\mathrm{DMI}}(\mathbf{q})$. By fitting the second term of Eq. (1) the DMI constants can be obtained. As for the exchange interaction, the DMI constants can be grouped in shells of intralayer and interlayer constants. Here we focus on magnetic states, which are close to the ferromagnetic ground state at $\mathbf{q} = 0$ and use an effective first-neighbor fit for each interaction. This means that we map all intralayer and interlayer contributions on nearest-neighbor DM interactions. However, we still distinguish between intra- and interlayer contributions. For the vector $\mathbf{D}$ from Eq. (1), we assume that it lies in the xy plane and is perpendicular to the connection between interacting atoms $\mathbf{R}_i - \mathbf{R}_j$ as sketched in Fig. 3(b). This assumption is consistent with the Levy-Fert model [38] for the given symmetry. For a flat cycloidal spin spiral propagating along $\mathbf{q}$ from the 2D-BZ this leads to the DMI energy term

$$E_{\mathrm{DMI}}(\mathbf{q}) = D_X^{||,1} \sum_j \sin(\mathbf{q}\mathbf{R}_j) + D_Y^{||,1} \sum_j \sin(\mathbf{q}\mathbf{R}_j) + D_{X-Y}^{\perp,1} \sum_j \sin(\mathbf{q}\mathbf{R}_j), \tag{5}$$

where the sums are performed for nearest-neighbor sites j. $D_X^{||,1}$ and $D_Y^{||,1}$ are the nearest-neighbor intralayer DMI constants and can be calculated from a spin spiral propagating only in the X or Y layer [cf. Figs. 2(b) and 2(c)]. When all spins in the other layer are oriented perpendicular to all spins of the spin spiral, the expression $\sum_{i,j} \mathbf{D}_{i,j}(\mathbf{m}_i \times \mathbf{m}_j)$ [cf. Eq. (1)] vanishes for interlayer component $D_{X-Y}^{\perp,1}$ with the assumed direction of the vector $\mathbf{D}$. The interlayer components can be calculated from a spin spiral propagating in both magnetic layers. In addition, we provide an effective DMI parameter D_{eff}, which treats the whole magnetic layer as one effective layer and allows a comparison with magnetic monolayer systems. Note that interlayer DMI can also occur between different magnetic layers separated by a nonmagnetic spacer [39–42]. In this case $\mathbf{D}$ cannot be assumed to lie in the xy plane [42]. We focus here on interlayer interaction within a magnetic bilayer since other investigations have shown that interlayer DMI over a spacer has a small contribution compared to the interfacial DMI [40].

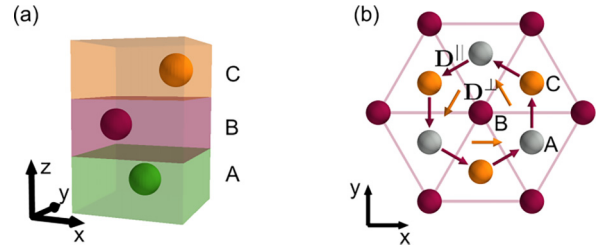

FIG. 3. (a) Side view of a multilayer system where for all layers the x and y components are displaced from the direct adjacent layers, such that the atoms are located in the hollow sides of adjacent layers. (b) Top view of the same structure as in (a). Each of the possible positions in the xy plane is referred to as a A, B, or C layer, which allows a unique definition of the stacking. The direction of DMI vectors for intralayer (interlayer) DMI are marked in red (yellow) for nearest neighbors.

3. Magnetocrystalline anisotropy

To calculate the MAE, the total energies of the ferromagnetic state with different orientations of the magnetization direction are calculated including SOC self-consistently [43]. In one configuration, all spins are pointing in the film plane of the magnetic layers, which yields E^{i}, and in the other case, they are all perpendicular to the plane, giving E^{o}. The MAE is defined as the total energy

difference $E_{\mathrm{MAE}} = E^{\mathrm{i}} - E^{\mathrm{o}}$ between the two configurations. In the atomistic spin model given by Eq. (1) the MAE is equivalent to the magnetocrystalline anisotropy constant K.

Note that in the long wave-length limit, i.e., small $|\mathbf{q}|$, a spin spiral state is by $K/2$ less favorable than the ferromagnetic alignment of all spins along the magnetic easy axis since on average half of the spins are orientated in-plane and half of the spins out-of-plane. The mean MAE contribution per spin for a spin spiral with N spins in one period is $\overline{E}_{\mathrm{MAE}} = \frac{K}{N}\sum_{i=1}^{N}(\mathbf{m}_i \cdot \mathbf{n})^2$ where $\mathbf{n}$ is the easy axis. The DMI favors a rotation around an axis within the surface plane, which is perpendicular to the spin spiral vector $\mathbf{q}$, resulting in a cycloidal spin spiral. Assuming an uniaxial anisotropy, the MAE of a cycloidal spin spiral is $\overline{E}_{\mathrm{MAE}} = K\frac{1}{2\pi}\int_0^{2\pi}\cos^2(\varphi)d\varphi = \frac{K}{2}$, since the alignment with the easy axis varies along one period of the spin spiral. Collinear magnetic states can align with $\mathbf{n}$ and have a MAE contribution of K. This makes spin spirals by $\frac{K}{2}$ less favorable than collinear states such as the FM state. The interplay of DMI and MAE is also discussed in Ref. [44].

In principle, the MAE contribution of each layer could be different. For the case of a very weak coupling of both layers, this might lead to different spin structures in each layer. As the exchange coupling between both layers is very strong compared to the MAE, we expect this effect to be negligible.

III. COMPUTATIONAL DETAILS

In this paper multilayers are compared to ultrathin films. Therefore, both types of systems should have the same geometric structure. The ultrathin film system Rh/Co/Ir(111) [Fig. 1(a)] is built on the Ir(111) surface, which determines the structure and in-plane lattice constant of the layers. This structure has been used here for the construction of the multilayers. Each atomic layer forms a hexagonal lattice with a distance of 2.70 Å between neighboring atoms as obtained from the theoretical lattice constant of Ir in local density approximation (LDA) as used in the reference system Rh/Co/Ir(111), which was investigated in Ref. [9].

In Fig. 3(a) three atomic layers of a multilayer are represented by different colors. Each layer forms a hexagonal sublattice. When two layers are stacked on top of each other, there are two possible positions denoted as B and C to place the atoms of one layer in the hollow sites of the other layer marked as A [Fig. 3(b)]. When stacking three layers on top of each other the stacking sequence could be either ABA or ABC, i.e., hcp or fcc stacking, respectively. The atomic layers can be grouped into the magnetic layers consisting of Co and Fe and the spacer layers consisting of Rh and Ir.

We consider multilayers built from an infinite repetition of a basic structure, e.g., a Rh/Co/Ir trilayer [Fig. 1(b)], in the direction perpendicular to the layers. Further, we vary the number n of spacer layers, Rh or Ir, in our calculations. We denote the multilayers by a sequence of the basic structure, e.g., Co/Rh(n) indicates a multilayer formed from the infinite repetition of one layer of Co and n layers of Rh. In a similar fashion, Rh(n)/Co/Fe/Ir(m) denotes a multilayer formed from the infinite repetition of n Rh layers, a Co/Fe bilayer, and m Ir layers.

Whereas all multilayer systems are set up as an infinite repetition of the unit cell, the Rh/Co/Ir(111) and Rh/Co/Rh(111) film systems were modeled by asymmetric films consisting of a Rh/Co bilayer on nine atomic layers of substrate and infinite vacuum regions on both sides. Further computational details of the ultrathin film systems can be found in Ref. [9] for Rh/Co/Ir(111) and in Ref. [45] for Rh/Co/Rh(111).

All DFT calculations were performed using the full-potential linearized augmented plane-wave (FLAPW) method as implemented in the FLEUR code [31]. For all calculations muffin-tin-radii of 2.3 a.u. were used for Rh and Ir atoms and 2.2 a.u. for Co and Fe atoms.

A. Structural relaxations

The distances of the atomic layers perpendicular to the magnetic plane (z direction) have been obtained from structural relaxations performed in the generalized gradient approximation (GGA) using the PBE exchange-correlation functional [46]. At first the z positions of all layers were relaxed for different sizes of the unit cell c. Then the unit-cell size c_0 with minimum energy $E(c_0) = \min E(c)$ was found by a cubic fit on the energy $E(c)$ over the size c in z direction. For the unit-cell size c_0 the z position of each layer was found by relaxation. The atomic positions have been considered as relaxed, when the forces on each atom were below 10^{-5} a.u. in z direction. Forces on the atoms in the plane were not considered. For all relaxations the collinear ferromagnetic state has been used. These relaxations have been performed for all considered systems except for Co/Rh(n) with $n \in \{3, 4, 5\}$. For these multilayers the relaxed interlayer distance between Co-Rh and Rh-Rh of the Co/Rh(2) system have been used to construct the unit cell. The cut-off parameter for the basis functions was set to $k_{\mathrm{max}} = 3.9\,\mathrm{a.u.}^{-1}$.

B. Spin spiral calculations

To obtain the exchange and DMI constants spin spiral calculations were performed. For these calculations the LDA exchange correlation functional [47] was used as in Ref. [9]. Clockwise and counterclockwise rotating cycloidal spin spirals are degenerate if SOC is neglected. In this case, the energy is calculated self-consistently based on the generalized Bloch theorem [32]. The DMI has been calculated using first-order perturbation theory [33,37] starting from the self-consistent charge density of the corresponding spin spiral in scalar-relativistic approximation [cf. Eq. (4)]. For all systems a cut-off parameter of $k_{\mathrm{max}} = 3.9\,\mathrm{a.u.}^{-1}$ was used. For a multilayer built from Rh/Co a $(25 \times 25 \times 14)$ **k**-point grid was used, for Rh/Co(2) a $(30 \times 30 \times 11)$ **k**-point grid, for Co/Rh(n) with $n \in \{3, 4, 5\}$ and Rh/Co/Ir a $(40 \times 40 \times 20)$ **k**-point grid, for Rh/Fe/Co/Ir and Rh/Co/Fe/Ir a $(33 \times 33 \times 9)$ **k**-point grid, for Rh(2)/Co/Fe/Ir(2) a $(37 \times 37 \times 7)$ **k**-point grid, and for Rh(2)/Co/Fe/Ir(3) a $(40 \times 40 \times 6)$ **k**-point grid.

C. Magnetocrystalline anisotropy energy

Because the MAE is a small quantity, a large number of **k** points and a high cut-off parameter $k_{\max}$ should be used for the calculations. We used $k_{max} = 4.5\,\text{a.u.}^{-1}$ and a large number of **k** points. For every system two collinear calculations in the ferromagnetic state were performed. In one calculation all spins were aligned within the plane of the atomic layers and in the other calculation perpendicular to this plane. Both calculations were performed self-consistently considering SOC using the second variational approach [43]. The used **k**-point sets were for Rh(2)/Co a $(43 \times 43 \times 16)$ **k**-point grid, for Rh/Co/Ir a $(54 \times 54 \times 20)$ **k**-point grid, for Rh/Fe/Co/Ir and Rh/Co/Fe/Ir a $(54 \times 54 \times 15)$ **k**-point grid, for Rh(2)/Co/Fe/Ir(2) a $(64 \times 64 \times 12)$ **k**-point grid and for Rh(2)/Co/Fe/Ir(3) a $(65 \times 65 \times 10)$ **k**-point grid.

IV. RESULTS

A. Rh/Co/Ir multilayer vs Rh/Co/Ir(111) film

It has been shown experimentally that Rh/Co/Ir(111) hosts sub-10 nm skyrmions at zero magnetic field, i.e., in the ferromagnetic ground state, which was explained based on DFT calculations and atomistic spin simulations [9]. Therefore, we begin by comparing the magnetic interactions in a multilayer built from an infinite repetition of Rh/Co/Ir trilayers with those of the film system of an atomic Rh/Co bilayer on the Ir(111) surface. Figure 4 shows the energy dispersion $E(\mathbf{q})$ of spin spirals for these two systems along the high symmetry direction $\overline{\text{M}} - \overline{\Gamma} - \overline{\text{K}}$ as sketched in Fig. 2(d). At the $\overline{\text{M}}$ point of the hexagonal Brillouin zone one obtains the row-wise antiferromagnetic (RW-AFM) state, at the $\overline{\Gamma}$ point the ferromagnetic (FM) state, and at the $\overline{\text{K}}$ point the Néel state, in which neighboring spins are canted by an angle of 120° with respect to each other.

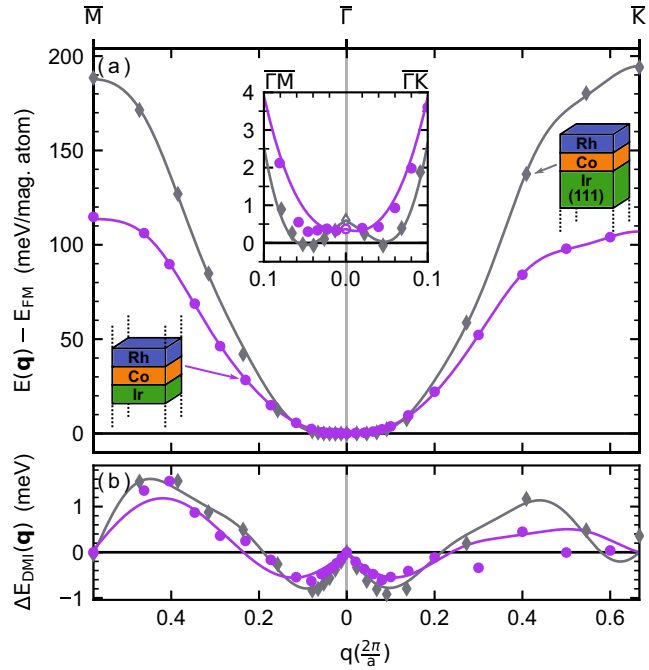

FIG. 4. Energy dispersion for spin spirals in the ultrathin film system Rh/Co/Ir(111) and in the multilayer built from Rh/Co/Ir trilayers along the high-symmetry direction $\overline{\text{M}} - \overline{\Gamma} - \overline{\text{K}}$ of the 2D-BZ. (a) Spin spiral energy dispersion $E(\mathbf{q})$ of scalar-relativistic calculations, i.e., neglecting SOC. (b) Energy contribution $\Delta E_{\text{DMI}}(\mathbf{q})$ to the spin spiral dispersion due to SOC for cycloidal spin spirals. In the inset in (a) all contributions are included, i.e., $E(\mathbf{q}) + \Delta E_{\text{DMI}}(\mathbf{q}) + K/2$, where K is the magnetocrystalline anisotropy energy. All energies are given with respect to the FM state at the $\overline{\Gamma}$ point. Symbols denote the values of DFT calculations and lines show a fit to the atomistic spin model. Note that in the inset of (a) the data points at $\overline{\Gamma}$ are not filled as the energy of the FM state is zero. The data for Rh/Co/Ir(111) were taken from Ref. [9].

1. Exchange interaction

From the energy dispersion $E(\mathbf{q})$ of flat spin spirals neglecting SOC [Fig. 4(a)] we obtain the exchange constants by a fit to the Heisenberg model, i.e., the first term of Eq. (1). In this system single Co layers are separated by a spacer. This simplifies Eq. (3) to $E^{\parallel}_{\text{Co}}(\mathbf{q})$. The interlayer contributions between the separated Co layers are evaluated in Appendix D.

An interesting feature seen in $E(\mathbf{q})$ is the energy difference between the FM state at the $\overline{\Gamma}$ point and the RW-AFM state at the $\overline{\text{M}}$ point. This energy difference is by about 70 meV per Co atom larger in the ultrathin film system than in the multilayer and it is approximately proportional to the nearest-neighbor-exchange constant J_1. A reason for the increase may be the fact that in the film system the Rh layer has an interface to the vacuum region while in the multilayer it is adjacent to Ir. In addition, there is an antiferromagnetic exchange coupling between adjacent Co layers across the Rh/Ir spacer layers (see Appendix D). The interlayer distances are also slightly different in the two systems: In Rh/Co/Ir(111) the interlayer distance between Rh and Co is around 1% smaller than in the multilayer system. Additionally, the distance between the Co layer and the Rh layer is around 3.6% higher. The reduced coordination at the surface compared to the multilayer affects the hybridization between the three elements and result in different binding distances. This affects the exchange interactions.

A key aspect of the energy dispersion in terms of exchange frustration is its curvature in the vicinity of the $\overline{\Gamma}$ point (FM state). For small length of the spin spiral vector $|\mathbf{q}| \leqslant 0.15 \times 2\pi/a$ the dispersions are very flat and similar for both film and multilayer system [Fig. 4(a)]. As shown previously for Rh/Co/Ir(111) [9], the energy dispersion $E(\mathbf{q})$ deviates strongly in this region from the expected parabolic q^2 behavior of a typical ferromagnet dominated by nearest-neighbor exchange. The reason for the deviation is the opposite sign of exchange constants of different shells, i.e., competing ferro- and antiferromagnetic coupling, which results in a frustration of interactions. Since both systems show a similar curvature around $\overline{\Gamma}$ (Fig. 4) they possess a similar exchange frustration. This effect can be quantified by the exchange constants which are summarized in Table I. The nearest-neighbor (NN) exchange constant, J_1, is ≈25.2 meV for the ultrathin film and ≈13.7 meV for the multilayer. The NN exchange is much larger than that with more distant neighbors and determines mainly the energy difference between the FM and the AFM state. Nevertheless, the exchange interaction is negative for

TABLE I. Exchange interaction constants obtained via DFT for the ultrathin film system Rh/Co/Ir(111) and several multilayers. A positive (negative) sign represents a ferromagnetic (antiferromagnetic) coupling. The interactions are given for nth-nearest-neighbor shells. The intralayer exchange interaction constants $J_{\mathrm{X}}^{||,n}$ are given for every magnetic layer X. For multilayers that contain a magnetic bilayer in the unit cell, the interlayer exchange constants $J_{\mathrm{X-Y}}^{\perp,n}$ are given between two magnetic layers X and Y. All values are given in meV per magnetic atom.

System	Interaction	$n=1$	2	3	4	5	6	7	8	9	10
Rh/Co/Ir(111)	$J_{\mathrm{Co}}^{||,n}$	25.18	0.25	−2.71	−0.63	−0.24	0.10	0.02	0.27	0.03	−0.28
Rh/Co/Ir	$J_{\mathrm{Co}}^{||,n}$	13.67	1.81	−1.53	−0.52	−0.29	−0.12	0.23	0.36	−0.01	−0.18
Rh/Co(2)/Ir	$J_{\mathrm{Co@Rh}}^{||,n}$	9.50	1.12	0.39	0.12						
	$J_{\mathrm{Co@Ir}}^{||,n}$	13.38	0.81	−1.24	0.34						
	$J_{\mathrm{Co\text{-}Co}}^{\perp,n}$	21.50	3.67	0.23	−0.45						
Rh/$\mathrm{Fe_{fcc}}$/Co/Ir	$J_{\mathrm{Co}}^{||,n}$	7.60	1.01	−0.32	0.09						
	$J_{\mathrm{Fe}}^{||,n}$	−0.50	−0.16	−0.57	0.14						
	$J_{\mathrm{Co\text{-}Fe}}^{\perp,n}$	15.37	6.78	−2.59	0.86						
Rh/$\mathrm{Fe_{hcp}}$/Co/Ir	$J_{\mathrm{Co}}^{||,n}$	9.06	−0.10	−0.74	−0.18						
	$J_{\mathrm{Fe}}^{||,n}$	1.15	0.82	−2.51	−0.17						
	$J_{\mathrm{Co\text{-}Fe}}^{\perp,n}$	9.64	0.37	0.78	0.18						
Rh/Co/$\mathrm{Fe_{hcp}}$/Ir	$J_{\mathrm{Co}}^{||,n}$	10.83	1.22	−0.51	0.11	−0.63					
	$J_{\mathrm{Fe}}^{||,n}$	0.47	0.38	−2.44	0.07	0.37					
	$J_{\mathrm{Co\text{-}Fe}}^{\perp,n}$	9.27	0.36	−0.27	−0.48	−0.43					
Rh(2)/Co/$\mathrm{Fe_{hcp}}$/Ir(2)	$J_{\mathrm{Co}}^{||,n}$	8.19	1.15	−0.78	0.11	−0.12					
	$J_{\mathrm{Fe}}^{||,n}$	0.26	0.05	−2.30	0.22	0.14					
	$J_{\mathrm{Co\text{-}Fe}}^{\perp,n}$	11.41	2.09	1.08	0.59	−1.07	−1.47	0.45	−0.09		

a number of beyond NN terms (Table I). In particular, the third NN exchange constant $J_3 < 0$ and the ratio of its absolute value with respect to the NN exchange $|J_3|/J_1 \approx 0.1$ is basically the same for both film and multilayer system, which indicates a similar exchange frustration.

2. *Dzyaloshinskii-Moriya interaction*

The energy contribution to cycloidal spin spirals due to DMI $\Delta E_{\mathrm{DMI}}(\mathbf{q})$ is similar for both systems [Fig. 4(b)]. The DMI is most important in the vicinity of the $\overline{\Gamma}$ point where the exchange energy is relatively small and varies little with $\mathbf{q}$. In this region, the magnitude of the DMI is slightly larger for the ultrathin film system. This is also reflected in the effective DMI constants D_{eff} (see Table II). D_{eff} originates from a fit of the second term in Eq. (1) with only a nearest-neighbor DMI constant to the region of $\Delta E_{\mathrm{DMI}}(\mathbf{q})$ close to the $\overline{\Gamma}$ point, which exhibits a linear variation of energy with $|\mathbf{q}|$. We obtain $D_{\mathrm{eff}} = 0.70$ meV for Rh/Co/Ir(111) and $D_{\mathrm{eff}} = 0.45$ meV for the multilayer Rh/Co/Ir. For completeness we give in Appendix E the DMI constants for a fit with up to seventh nearest neighbors.

The increased effective DMI in the ultrathin film is plausible since it is mediated by the atoms with a high spin-orbit coupling, in this case mainly Ir. For the ultrathin film system, there are more Ir layers, whereas in the multilayer system there is only one, which leads to a smaller DMI. The closest Ir layer should have the highest contribution, which can explain that the difference in DMI between the two systems is not very large. In both systems the effective DMI constant is positive, which denotes a favored clockwise rotational sense.

3. *Magnetic ground state*

The inset in Fig. 4(a) shows the energy dispersion of clockwise rotating cycloidal spin spirals including exchange, DMI, and the magnetocrystalline anisotropy energy. Note the very small rise of energy up to values of $|\mathbf{q}| = 0.1 \times 2\pi/a$ and that the energy dispersion of all spin spiral states is shifted by half of the magnetocrystalline anisotropy energy $K/2$, with respect

TABLE II. DMI constants for the ultrathin film system Rh/Co/Ir(111) and selected multilayer systems. An effective DMI constand D_{eff} is given, which treats the whole magnetic layer as one effective layer and allows comparison of magnetic monolayer and bilayer systems. Further, for bilayer systems the DMI is divided into intra- and interlayer contributions. The intralayer contributions $D^{||,1}$ give the DMI strength in one atomic layer for nearest neighbors. The interlayer contribution $D^{\perp,1}$ gives the interaction between nearest neighbors in two adjacent atomic layers. The index X (Y) represents the first (second) magnetic layer of the system. For example, in Rh/$\mathrm{Fe_{hcp}}$/Co/Ir X represents the Fe layer and Y the Co layer. For the fit of all constants only the linear region of the DFT total energies around the $\overline{\Gamma}$ point was used. All values are given in meV per magnetic atom.

System	D_{eff}	$D_{\mathrm{X}}^{||,1}$	$D_{\mathrm{Y}}^{||,1}$	$D_{\mathrm{X\text{-}Y}}^{\perp,1}$
Rh/Co/Ir(111)	0.70			
Rh/Co/Ir	0.45			
Rh/Co(2)/Ir	−0.25	−0.18	−0.38	0.43
Rh/$\mathrm{Fe_{fcc}}$/Co/Ir	−0.15	−0.24	−0.27	0.46
Rh/$\mathrm{Fe_{hcp}}$/Co/Ir	−0.21	0.76	−0.65	−0.41
Rh/Co/$\mathrm{Fe_{hcp}}$/Ir	1.50	−0.31	0.87	1.19
Rh(2)/Co/$\mathrm{Fe_{hcp}}$/Ir(2)	2.31	0.30	0.66	2.14

to the FM state at the $\overline{\Gamma}$ point. From the inset one can see that the ground state of the multilayer system Rh/Co/Ir is the FM state at zero energy, while a spin spiral is slightly below zero for the ultrathin film Rh/Co/Ir(111). Since in Rh/Co/Ir(111), stable magnetic skyrmions have been observed and explained by the flat curvature of the energy dispersion [9], we expect skyrmions to occur similarly in the multilayer system.

B. Rh/Co/Co/Ir vs Rh/Co/Fe/Ir or Rh/Fe/Co/Ir multilayers

As a next step, we study whether the strong exchange frustration of the Rh/Co/Ir multilayer can be transferred to a multilayer with two magnetic layers. The bilayer systems can be ordered in three groups: In the first type, the bilayer consists of two atomic Co layers, while in the other two types, the bilayer consists of one Co and one Fe layer. Within the Co/Fe bilayer systems, we can distinguish bilayers with a local fcc or hcp environment around the Fe layer. Our calculations show that the local stacking sequence of the Fe layer is much more important than that around the Co layer.

1. Exchange interaction

We explore the exchange interactions in these systems by focusing on total energy calculations neglecting SOC. The energy dispersions of spin spirals propagating in both magnetic layers are shown for different multilayers in Fig. 5 where for each of the three bilayer types one system is presented. The energy dispersions of more systems of each category have been calculated. They behave qualitatively similar and are presented in Appendix C (Fig. 14).

For the system with a Co bilayer, i.e., Rh/Co(2)/Ir, the energy at the $\overline{\mathrm{M}}$ point is much higher than for all other systems and the dispersion rises more steeply close to the $\overline{\Gamma}$ point [Fig. 5(a)]. Therefore, the FM state is energetically clearly favorable with respect to noncollinear states.

Compared to the Co-bilayer system all multilayers with a Co/Fe bilayer exhibit a higher exchange frustration, which results in the flatter curvature of $E(\mathbf{q})$ around the $\overline{\Gamma}$ point [inset of Fig. 5(a)]. The multilayer built from the infinite repetition of Rh/$\mathrm{Fe_{fcc}}$/Co/Ir quadlayers, with a local fcc environment of the Fe layer, exhibits a comparably small energy rise close to the FM state making it interesting for further investigations. The multilayer Rh/Co/$\mathrm{Fe_{hcp}}$/Ir, with a local hcp environment of the Fe layer, has an even flatter energy dispersion, which is quantitatively comparable to that of the Rh/Co/Ir multilayer [cf. Fig. 4(a)]. In general, we find from our DFT calculations that systems with a local hcp stacking around the Fe layer exhibit a higher exchange frustration than systems with a local fcc stacking (cf. Fig. 14 in Appendix C).

The magnetic moment of Fe is relatively unaffected by a variation of the spin spiral vector $\mathbf{q}$ [Fig. 5(b)]. The Fe moment is considerably higher in the local fcc stacking compared to the hcp stacking [Fig. 5(b)]. This indicates a change of the hybridization with the adjacent Ir layer. It has been found previously that the hybridization at the Fe/Ir interface strongly affects the exchange interaction in the Fe layer [10,48–51]. The Co magnetic moment varies more as a function of $\mathbf{q}$ in line with previous studies [9]; however, it is less affected by the Co/Ir vs Co/Rh interface or the local stacking sequence.

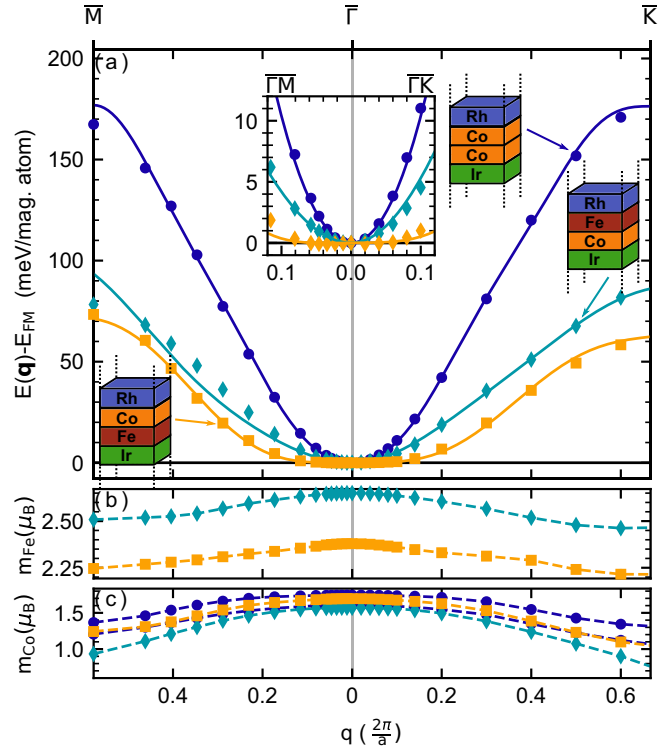

FIG. 5. (a) Energy dispersions $E(\mathbf{q})$ and [(b),(c)] magnetic moments for spin spirals calculated in the scalar-relativistic approximation, i.e., neglecting SOC, for the multilayers Rh/Co(2)/Ir, Rh/$\mathrm{Fe_{fcc}}$/Co/Ir, Rh/Co/$\mathrm{Fe_{hcp}}$/Ir [see sketches in (a)] along the high-symmetry direction $\overline{\mathrm{M}}-\overline{\Gamma}-\overline{\mathrm{K}}$. Symbols denote DFT data. Lines in (a) show the fit to the Heisenberg model. The lines in (b) and (c) are a guide to the eye. All energies are given with respect to the FM state at $\overline{\Gamma}$. The magnetic moments for (b) Fe and (c) Co atoms are given for each spin spiral state. The inset in (a) shows a zoom of the energy dispersion at the region around the $\overline{\Gamma}$ point.

2. Inter- vs intralayer exchange

In order to understand why the exchange frustration differs so much between multilayers with Co bilayers and Co/Fe bilayers (Fig. 5) we have performed spin spiral calculations in which the spiral propagates only in one of the magnetic layers while the magnetic moments of the other layer are aligned parallel with respect to each other and perpendicular to the rotation plane of the spin spiral in the other layer [cf. Figs. 2(b) and 2(c)]. Figure 6 shows the corresponding energy dispersions obtained for four considered multilayer systems in comparison to that of spin spirals propagating in both layers [cf. Fig. 2(a)].

For the multilayer with the Co bilayer, Rh/Co(2)/Ir [Fig. 6(a)], we find that spin spirals propagating either in the Co layer adjacent to the Ir layer (Co@Ir) or adjacent to the Rh layer (Co@Rh) display very similar energy dispersions. This is consistent with the expectation since Rh and Ir are isoelectronic 4*d* and 5*d* transition metals. However, the sum of the single spin spiral energy dispersions (green curve) deviates significantly from that obtained by a calculation for a spin spiral propagating in both Co layers (blue symbols and curve). As explained in Sec. II the difference between these two dispersions gives the interlayer exchange interaction

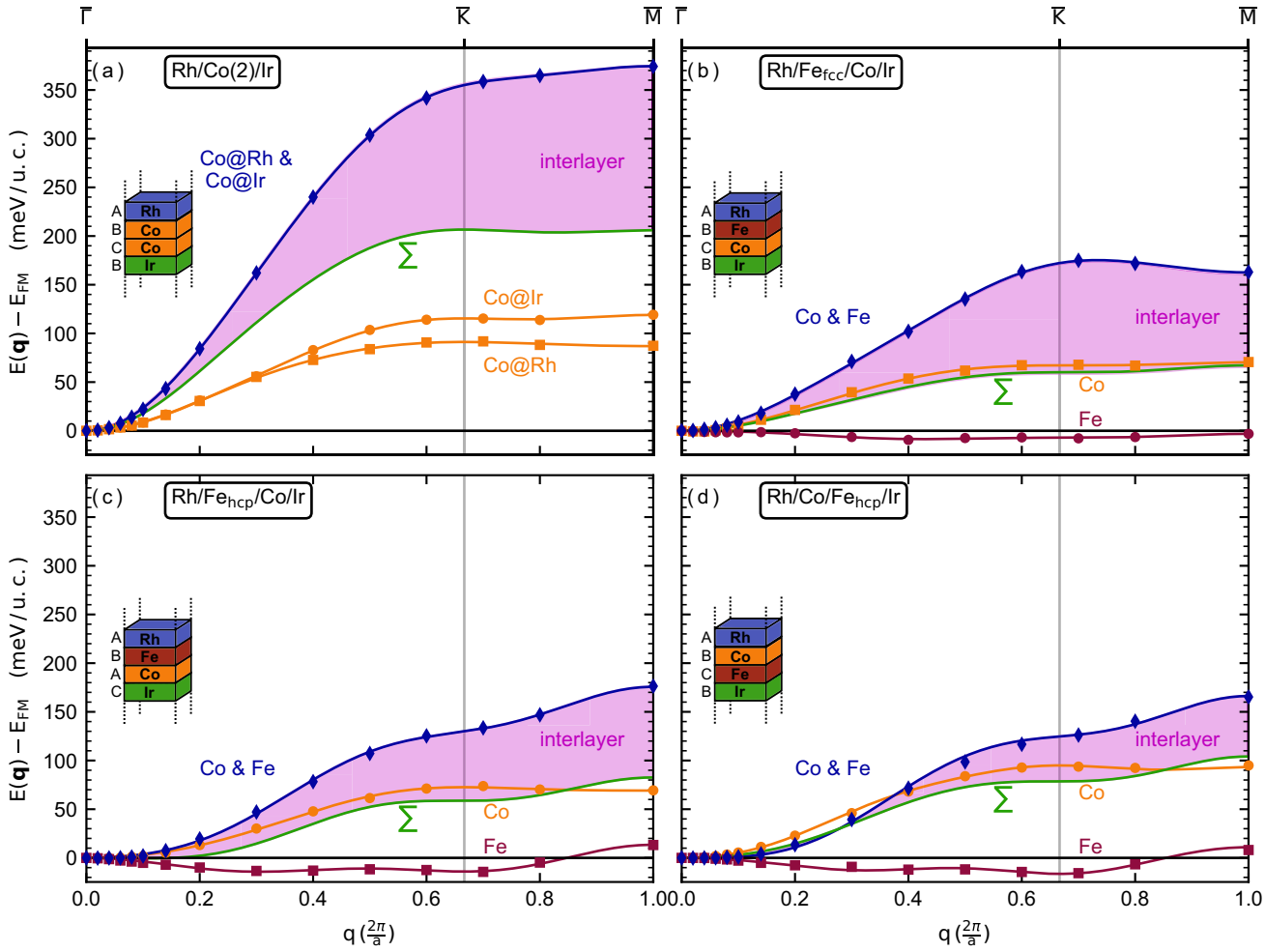

FIG. 6. Energy dispersions $E(\mathbf{q})$ for spin spirals in multilayers with (a) a Co/Co bilayer or [(b)–(d)] a Co/Fe bilayer along the high-symmetry direction $\overline{\Gamma} - \overline{\mathrm{K}} - \overline{\mathrm{M}}$. The atomic layers and the stacking sequence for each multilayer is shown as an inset in each panel. The energy dispersions are displayed for spin spirals [cf. Figs. 2(a)–2(c)] propagating in both magnetic layers (blue), only in one Co layer (orange), or only in the Fe layer (red). Symbols denote DFT total energies in meV per unit cell (u.c.) calculated in the scalar-relativistic approximation, i.e., without SOC, and lines are a fit to the Heisenberg model. The sum of the energy dispersions in the Co and in the Fe layer [or second Co layer in panel (a)] are given as the green curve. The difference between the sum and the energy of a spin spiral propagating in both layers gives the interlayer interaction, which is displayed in purple. Circles indicate a magnetic layer with an interface to an Ir layer and squares an interface to a Rh layer.

$J^{\perp}_{\mathrm{Co-Co}}$. This is represented as a purple area between the two curves.

For all Co/Fe bilayer-based multilayer systems [Figs. 6(b)–6(d)] the energy dispersion of spin spirals only in the Co layer [orange curve in Figs. 6(b)–6(d)] is very similar to that in the Co bilayer [Fig. 6(a)] and exhibits a minimum at $\mathbf{q} = 0$, i.e., the FM state. In contrast, for spin spirals propagating only in the Fe layer [red curve in Figs. 6(b)–6(d)] a state with a finite value of q is energetically lowest for all investigated Co/Fe-bilayer systems. This is consistent with the spin spiral ground state found for the film system Rh/Fe/Ir(111) [51].

The qualitatively different energy dispersions of spin spirals propagating only in the Fe layer or in the Co layer explains why the energy dispersion of spirals propagating in both layers is very different for multilayers based on Co/Fe bilayers vs those with a Co bilayer (cf. Fig. 5). In particular, the energy dispersions of spin spirals in the Co/Fe bilayers show a flatter trend close to the $\overline{\Gamma}$ point. In addition, the interlayer exchange interaction is smaller for Co/Fe bilayers than for the Co bilayer. The interlayer interactions between both atomic layers are ferromagnetic in all four systems. This can be seen from the exchange constants in Table I. The major contributions have a positive sign. For the Rh/Co(2)/Ir system [Fig. 6(a)] the two Co layers favor a ferromagnetic alignment to each other and spin spirals propagating only in one of the Co layers also favor a ferromagnetic state. In contrast, in the Co/Fe-bilayer systems [Fig. 6(b)–6(d)] two atomic layers are coupled ferromagnetically, which prefer different spin states. This leads to a high exchange frustration in the Co/Fe bilayer.

There are some small differences among the multilayers containing a Co/Fe magnetic bilayer. For some of the systems a frustration exists even in the exchange interaction between the Co and the Fe layer. This can be seen from the interlayer exchange constants $J^{\perp}_{\mathrm{Co-Fe}}$ given in Table I. The effect

is particularly clear for the system Rh/Fe_{fcc}/Co/Ir. Here we find $J^{\perp}_{Co-Fe,1} \approx 15.37$ meV and $J^{\perp}_{Co-Fe,3} \approx -2.59$ meV. This results in an additional frustration in the bilayer.

Both of the Co/Fe-bilayer based multilayers with a local hcp stacking around the Fe layer, namely Rh/Fe_{hcp}/Co/Ir [Fig. 6(c)] and Rh/Co/Fe_{hcp}/Ir [Fig. 6(d)], exhibit a deeper energy minimum in the Fe layer, than Rh/Fe_{fcc}/Co/Ir [Fig. 6(b)]. This comes along with increased hybridization at the interface and smaller magnetic moments of these systems as shown in Figs. 5(b) and 5(c). In addition, the magnitude of the interlayer exchange coupling, represented by the purple area in Fig. 6, between both atomic layers is smaller for hcp than for fcc systems.

The multilayers with a local hcp environment, Rh/Fe_{hcp}/Co/Ir and Rh/Co/Fe_{hcp}/Ir, behave qualitatively very similar. There are some minor influences from the interface between the magnetic and the spacer layers, but qualitatively the energy dispersion does not change as expected since Ir and Rh are isoelectronic elements. We conclude that a Co/Fe bilayer sandwiched between Ir and Rh layers exhibits a high exchange frustration due to the different intralayer exchange constants in the Co and the Fe layer. A local hcp stacking around the Fe layer further enhances this frustration.

The exchange interactions discussed up to this point describe the behavior within a magnetic mono- or bilayer. An important aspect of multilayers is the exchange coupling between the magnetic mono- or bilayers [cf. Figs. 1(b), 1(c)]. Depending on the sign of the exchange constants adjacent magnetic layers can couple ferro- or antiferromagnetically. Concerning magnetic skyrmions it has been proposed to use synthetic antiferromagnets [20], which exhibit favorable transport properties such as the absence of the skyrmion Hall effect.

We have calculated the strength of the interlayer exchange interaction for the multilayers considered in our paper as a function of the number of nonmagnetic spacer layers (see Appendix D). We find that multilayers with only two atomic spacer layers possess a very strong interlayer coupling with an energy difference between the FM and AFM coupling of adjacent layers of about 10 to 50 meV/magnetic atom, while it is only a few meV for three or more spacer layers. In most of the multilayers, the sign of the interlayer exchange favors an antiferromagnetic coupling between adjacent magnetic mono- or bilayers (for details see Appendix D).

3. *Dzyaloshinskii-Moriya interaction*

Now we turn to the DMI in the multilayers with a Co bilayer or a Co/Fe bilayer. We consider only the DMI within the bilayer due to the interfaces with the adjacent nonmagnetic Rh and Ir layers as described in Sec. II. A possible interlayer DMI between adjacent magnetic bilayers mediated by spacer layers (such as in Refs. [39–42]) is neglected here since for multilayers with two or more atomic spacer layers it is not expected to be significant and already the interfacial DMI is small compared to the exchange interactions.

In Fig. 7 the DMI contribution to the energy of cycloidal spin spirals, $\Delta E_{DMI}(\mathbf{q})$, is shown along the high-symmetry direction $\overline{\Gamma} - \overline{K}$ for selected multilayers. A similar plot is obtained along the $\overline{\Gamma} - \overline{M}$ direction (not shown). We focus

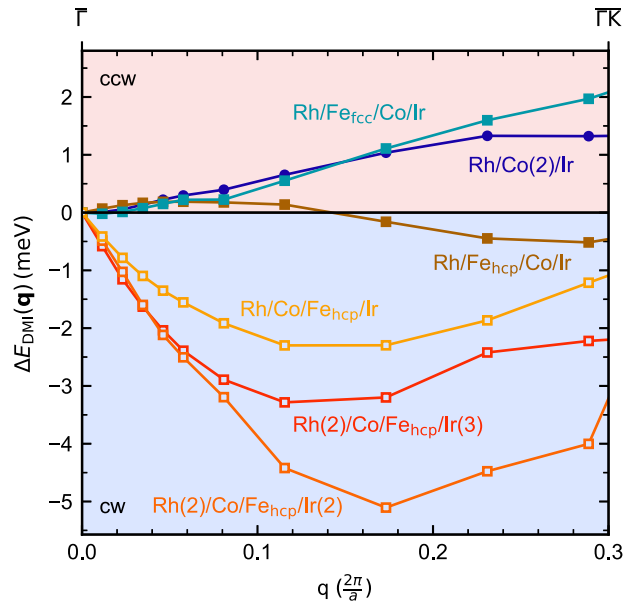

FIG. 7. Energy contribution $\Delta E_{DMI}(\mathbf{q})$ due to SOC for selected multilayers to the energy dispersion of cycloidal spin spirals along the high-symmetry direction $\overline{\Gamma K}$ propagating in both magnetic layers of the bilayer. Symbols show the total DFT energies per unit cell. Filled squares denote multilayers with a Co/Ir and an Fe/Rh interface, while open squares are used for multilayers with a Co/Rh and a Fe/Ir interface. The circles represent a system with a Co bilayer. The lines are a guide to the eye. Negative (positive) values denote a favored clockwise (counter-clockwise) rotational sense.

on the vicinity of the $\overline{\Gamma}$ point in which the DMI contribution is most relevant for the total energy dispersion since the magnetic ground state occurs for small values of $|\mathbf{q}|$ (see also Sec. V). A negative sign denotes a favored clockwise (cw) rotational sense and a positive sign a favored counter-clockwise (ccw) rotational sense of the respective cycloidal spin spiral state.

The DMI energy of multilayers, which possess a Co/Ir and an Fe/Rh interface is positive close to $\overline{\Gamma}$ and thus a counterclockwise rotational sense is preferred. In contrast, all Co/Fe-bilayer systems with a Co/Rh and an Fe/Ir interface favor a clockwise rotational sense. In addition, the absolute value of the DMI contribution is much larger for the latter systems. Both effects can be attributed to the strong DMI at the Fe/Ir interface as we will show below.

To understand the change of the rotational sense upon switching the Co/Rh and Fe/Ir interfaces, we analyze the contributions of the Ir and Rh layers to the total DMI energy (Fig. 8). The largest part of the DMI energy arises in the mediating layer with a strong SOC constant, here Ir and Rh, and not in the magnetic 3*d* transition-metal layers [52]. Therefore, the contributions of the Fe and Co layer are small and not shown here for clarity of the figure. As a reference, the multilayer Rh/Co_{fcc}/Ir with a single magnetic (Co) layer within the unit cell is given in Fig. 8(a). The contributions of Rh and Ir to the DMI have an opposite sign. This can be understood based on the fact that one layer is above the magnetic layer and one is underneath it. From their point of view both layers prefer the same rotational sense, but due

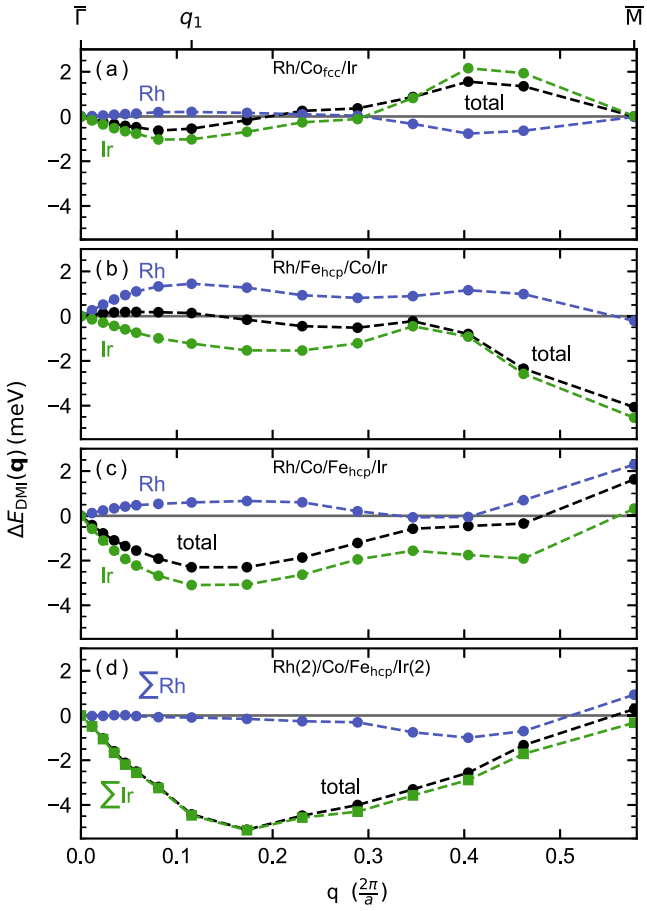

FIG. 8. Atom-resolved DMI energy contribution $\Delta E_{\mathrm{DMI}}(\mathbf{q})$ to the spin spiral energy dispersion along the high-symmetry direction $\overline{\Gamma\mathrm{M}}$ for selected multilayers. The cycloidal spin spirals are propagating in both magnetic layers of the bilayer: (a) Rh/Co/Ir, (b) Rh/Fe$_{\mathrm{hcp}}$/Co/Ir, (c) Rh/Co/Fe$_{\mathrm{hcp}}$/Ir, and (d) Rh(2)/Co/Fe$_{\mathrm{hcp}}$/Ir(2). The black circles show the total DMI energy while the green (blue) circles represent the DFT energy from all Ir (Rh) layers. The spin spiral vector q_1 used in Fig. 9 is marked.

to one interface being turned upside down the contributions have opposite signs. The absolute value of the contribution is higher for Ir than for Rh, which is a result of the much larger SOC constant of the heavy 5*d* transition-metal Ir compared to the isoelectronic 4*d* element Rh. The total DMI follows the contribution from the dominating Ir layer.

For the multilayer Rh/Fe$_{\mathrm{hcp}}$/Co/Ir with an Fe/Rh and a Co/Ir interface [Fig. 8(b)], Rh has a contribution to the DMI of the same order as that of Ir. Therefore, the Rh and Ir contributions can compete and the sign of the total DMI is positive close to the $\overline{\Gamma}$ point. In contrast in Rh/Co/Fe$_{\mathrm{hcp}}$/Ir with a Co/Rh and an Fe/Ir interface [Fig. 8(c)], the contribution of Ir is much larger than of Rh and the Ir contribution dominates the total DMI energy. Thus the contribution of Ir decreases, when switching from an interface with Fe to a Co interface [from panel (c) to (b)]. At the same time the contribution of Rh is increased, when switching from an interface with Co to an interface with Fe. This fits qualitatively to the atomistic spin model, in which the DMI energy depends on the magnetic moments of the coupled atoms. Because Fe has a higher magnetic moment than Co (cf. Fig. 5), the DMI energy of the interface with this layer dominates. In the case of Rh/Fe$_{\mathrm{hcp}}$/Co/Ir vs Rh/Co/Fe$_{\mathrm{hcp}}$/Ir this leads to a different rotational sense of the lowest energy spin spiral (cf. Fig. 7).

Figure 8(d) shows the DMI contributions to the spin spiral energy dispersion for Rh(2)/Co/Fe$_{\mathrm{hcp}}$/Ir(2). This multilayer favors the same rotational sense as Rh/Co/Fe$_{\mathrm{hcp}}$/Ir because it also possesses an Fe/Ir and a Co/Rh interface. However, the DMI contribution of the Rh layers is reduced while the Ir contribution is significantly enhanced. This explains the overall increase of the DMI energy observed in Fig. 7. This result is consistent with the observations in Sec. A that the DMI of the ultrathin film system Rh/Co/Ir(111) with an Ir substrate is stronger than for the multilayer system Rh/Co/Ir with just a single layer of Ir.

Our analysis shows that the type of 3*d*/4*d* or 3*d*/5*d* interface is decisive for the strength of the DMI and its favored rotational sense. In order to obtain a deeper insight into how the interfaces lead to the DMI contributions we study the electronic structure of the multilayers. Figure 9 displays the local density of states (LDOS) of the Co and Fe layers as well as the adjacent Rh and Ir layers for the Rh/Fe$_{\mathrm{hcp}}$/Co/Ir, the Rh/Co/Fe$_{\mathrm{hcp}}$/Ir, and the Rh(2)/Co/Fe$_{\mathrm{hcp}}$/Ir(2) multilayer. We compare the LDOS of the FM state ($\mathbf{q} = 0$) with that of a spin spiral state with a wave vector along the $\overline{\Gamma\mathrm{M}}$ direction with an absolute value of $q_1 \approx 0.11 \times \frac{2\pi}{a}$ (cf. Fig. 8).

The LDOS of the Co and Fe layers displays the exchange splitting between majority and minority spin bands. The splitting is larger for Fe than for Co as expected from the larger Fe magnetic moment. Due to the hybridization at the interfaces, the LDOS of the Rh and Ir layer are also spin-polarized leading to small induced magnetic moments. Since Rh and Ir are isoelectronic 4*d* and 5*d* elements their LDOS is similar but the bandwidth increases for Ir. The hybridization between different layers is apparent by peaks in the LDOS at the same energy and of similar shape. One can also observe that the LDOS of the magnetic layers is considerably affected by the type of interface [cf. Figs. 9(d) and 9(h) or Figs. 9(e) and 9(g)]. Upon increasing the number of Rh and Ir layers, the LDOS at the Rh and Ir interface layers [Figs. 9(c) and 9(l)] is modified due to the hybridization with the additional nonmagnetic layers. The LDOS of the spin spiral state exhibits spin mixing, which is visible from peaks in the Fe and Co LDOS appearing at the same energy in the spin-up and spin-down channel.

The energy contribution due to SOC to the dispersion of a spin spiral state with wave vector $\mathbf{q}$ is given for a single $\mathbf{k}$ point by $\delta\epsilon_{\mathbf{k},\nu}(\mathbf{q})$ obtained by first-order perturbation theory [cf. Eq. (4)]. We can obtain an energy-dependent quantity analogous to the LDOS by summing over the band index ν and performing an integration over the 2D BZ,

$$\epsilon_{\mathrm{SOC}}(E, \mathbf{q}) = \sum_{\nu} \int_{\mathrm{2DBZ}} \delta\epsilon_{\mathbf{k},\nu}(\mathbf{q})\, \delta(E - E_{\mathbf{k},\nu}) d^2k. \quad (6)$$

Since $\delta\epsilon_{\mathbf{k},\nu}(\mathbf{q})$ is calculated within the muffin-tin spheres, one can calculate $\epsilon_{\mathrm{SOC}}(E, \mathbf{q})$ separately for the different atoms as shown in Figs. 9(m)–9(p) for the three considered multilayers. As for the atom-resolved DMI energy (Fig. 8) only the Ir and Rh layer contributions are displayed.

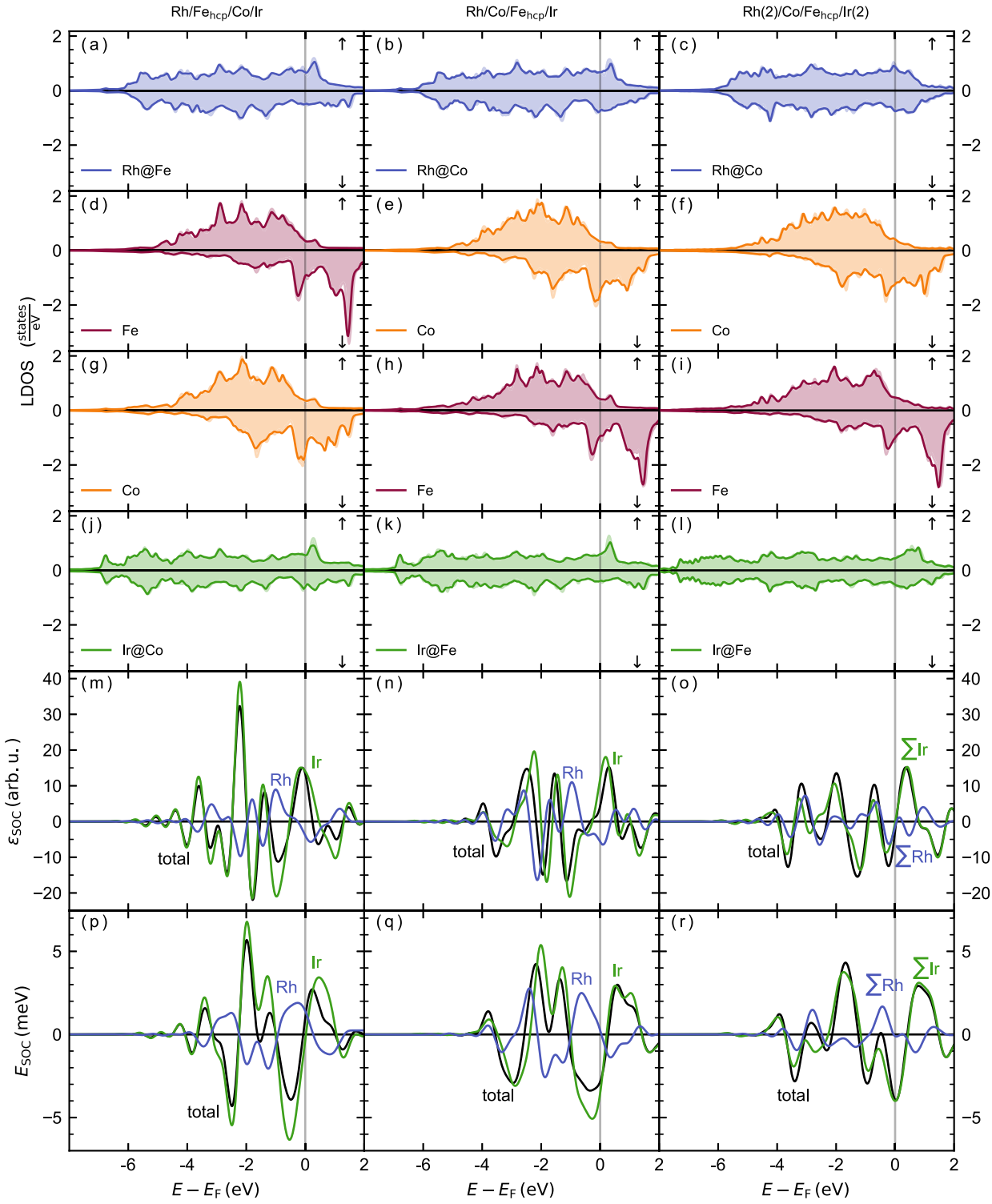

FIG. 9. [(a)–(l)] Spin-resolved local density of states (LDOS) of the multilayers Rh/Fe$_{hcp}$/Co/Ir, Rh/Co/Fe$_{hcp}$/Ir, and Rh(2)/Co/Fe$_{hcp}$/Ir(2). The LDOS is given for the atoms of the magnetic layer, Co and Fe, and the atoms of the spacer layer, Rh and Ir, which are adjacent to the magnetic layer. The filled areas denote the LDOS for $q = 0$ (FM state) and the lines represent the LDOS for a spin spiral state with $q_1 \approx 0.11 \times \frac{2\pi}{a}$ along the $\overline{\Gamma M}$ direction (cf. Fig. 8). [(m)–(o)] Contribution to the DMI energy $\epsilon_{SOC}(E, \mathbf{q})$ for the spin spiral state with q_1 [cf. Eq. (6)] for Ir layers (green), Rh layers (blue), and total contribution (black). [(p)–(r)] Integrated contribution to the DMI energy $E_{SOC}(E, \mathbf{q})$ for the spin spiral state with q_1 [cf. Eq. (7)] for Ir layers (green), Rh layers (blue), and total contribution (black).

Both Rh and Ir exhibit positive and negative contributions and the total curve follows that of the dominating Ir term [Figs. 9(m)–9(o)]. One can notice a prominent peak in the Ir curve at the Fermi energy E_F with a positive contribution [Fig. 9(m)], which shifts above E_F upon switching the stacking in the magnetic bilayer to Rh/Co/Fe/Ir [Fig. 9(n)]. Upon adding a Rh and an Ir layer [Fig. 9(o)] the peak is completely above the Fermi energy. This shift is responsible for the change of sign of the DMI contribution seen in Figs. 8(b)–8(d) as we will show below.

To obtain the DMI contribution to the energy of the spin spiral with a given wave vector $\mathbf{q}$ one needs to integrate $\epsilon_{SOC}(E, \mathbf{q})$ for all occupied states, i.e., up to E_F. We can perform the energy integration up to an arbitrary energy E in order to study the dependence on the location of the Fermi level,

$$E_{SOC}(E, \mathbf{q}) = \int_{-\infty}^{E} \epsilon_{SOC}(E', \mathbf{q})\, dE'. \tag{7}$$

Since $\epsilon_{SOC}(E, \mathbf{q})$ varies in sign the integrated contribution $E_{SOC}(E, \mathbf{q})$ vanishes at certain energies [Figs. 9(p)–9(r)]. The integrated contribution $E_{SOC}(E_F, \mathbf{q})$ at the Fermi energy defines the DMI contribution and can be directly compared to the values of $\Delta E_{DMI}(\mathbf{q})$ presented in Fig. 8 for the respective spin spiral vector $\mathbf{q}$. The peak close to E_F observed in $\epsilon_{SOC}(E, \mathbf{q})$ [Figs. 9(m)–9(o)] leads to a very steep rise of $E_{SOC}(E, \mathbf{q})$ in the vicinity of the Fermi energy. For the multilayers Rh/Fe_{hcp}/Co/Ir and Rh/Co/Fe_{hcp}/Ir, the rise is located directly at E_F and leads to a slightly positive value for the former and to a negative value of the DMI energy $E_{SOC}(E_F, \mathbf{q})$ for the latter system. For the multilayer Rh(2)/Co/Fe_{hcp}/Ir(2), $E_{SOC}(E, \mathbf{q})$ has a local minimum at the Fermi energy due to the shift of the peak in $\epsilon_{SOC}(E, \mathbf{q})$ above E_F. This leads to the large DMI and makes this system and its DMI more robust against small changes in the hybridisation.

The energy resolved analysis of the contributions to the DMI energy shows how the hybridization at the interfaces of the Fe and Co layer with the nonmagnetic Rh and Ir layers can lead to the change of DMI observed in Fig. 7. A shift of states at the Fermi energy can be decisive due to the steep variation of the contributions with energy.

4. Inter- vs intralayer DMI

So far we discussed qualitatively how the spacer material and the interface with the magnetic layer affects the DMI. In the following, we explore in how far one can define inter- and intralayer DMI constants for the two magnetic layers, which could be used within an atomistic spin model. Starting from the self-consistent spin spiral calculations used to obtain intra- and interlayer exchange interaction constants (Fig. 6), we calculated the SOC contributions to the energy dispersions using Eq. (4). In Fig. 10 these SOC contributions $\Delta E_{DMI}(\mathbf{q})$ are displayed for the multilayers Rh/Co(2)/Ir, Rh/Fe_{hcp}/Co/Ir, Rh/Co/Fe_{hcp}/Ir, and Rh(2)/Co/Fe_{hcp}/Ir(2).

By calculating $\Delta E_{DMI}(\mathbf{q})$ for cycloidal spin spirals propagating only in one of the two magnetic layers [cf. Figs. 2(b) and 2(c)] the intralayer Co and Fe DMI contributions are obtained. The sum of these two energy contributions (green curve in Fig. 10) should result in that calculated for a spin

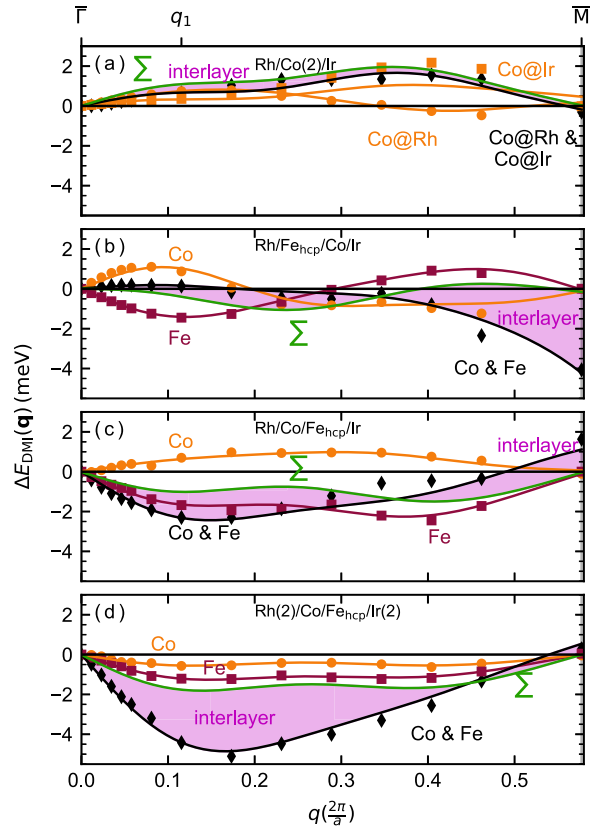

FIG. 10. Total DMI energy contributions $\Delta E_{DMI}(\mathbf{q})$ to the spin spiral energy dispersion along the high-symmetry direction $\overline{\Gamma M}$ for selected multilayers: (a) Rh/Co(2)/Ir, (b) Rh/Fe_{hcp}/Co/Ir, (c) Rh/Co/Fe_{hcp}/Ir, and (d) Rh(2)/Co/Fe_{hcp}/Ir(2). The spin spirals are propagating in both magnetic layers of the bilayer, cf. Fig. 2(a) or in one of the layers [red and orange, cf. Figs. 2(b) and 2(c)]. The green line represents the sum of energies for spin spirals in the individual layers (sum of red and orange curve) and the purple area shows the contribution of interlayer DMI in the bilayer.

spiral propagating in both magnetic layers [black dots and curve, cf. Fig. 2(a)] if the DMI is simply the sum of these two intralayer terms. While these two curves are very similar for the Rh/Co(2)/Ir multilayer [Fig. 10(a)], significant differences appear for the other three systems. These differences can be mapped to interlayer DMI constants. Note that here interlayer DMI means DMI between directly adjacent atomic layers of the magnetic material, which are not separated by a spacer as described in Sec. II.

The importance of the interlayer DMI can clearly be seen at the $\overline{M}$ point for Rh/Fe_{hcp}/Co/Ir [Fig. 10(b)]. The total DMI has a significant contribution at this point. But each layer is in the RW-AFM state, which results in zero intralayer DMI as all spins within the layer are collinear. Nevertheless, there is a tilting of the spins between the layers. Thus this contribution can only be explained by interlayer DMI. All considered systems exhibit an interlayer DMI contribution on the order of the DMI contribution of the individual layers (cf. values in Table II). For Rh(2)/Co/Fe_{hcp}/Ir(2) [Fig. 10(d)] the interlayer contribution is even larger than the intralayer contributions. For the two systems Rh/Co(2)/Ir [Fig. 10(a)] and Rh(2)/Co/Fe_{hcp}/Ir(2) both intralayer contributions favor

the same rotational sense, while they have opposite signs for $Rh/Fe_{hcp}/Co/Ir$ and $Rh/Co/Fe_{hcp}/Ir$. This is a result of the competing contributions of the spacer layers Rh and Ir for each individual layer.

The intralayer as well as the interlayer contributions to the DMI show signs of frustration (cf. Fig. 10). However, for simplicity we have used only data points up to $|\mathbf{q}| \leqslant 0.1 \times \frac{2\pi}{a}$ for an effective nearest-neighbor fit of the DMI. The fit parameters for selected multilayer systems are given in Table II. Here also an effective DMI constant D_{eff} is given using the same range of q values but treating the bilayer effectively as a single magnetic layer. For systems with only a single Co layer as the magnetic layer, the effective DMI constant is equal to the intralayer constant and an interlayer constant does not exist.

For the Rh/Co(2)/Ir multilayer, both intralayer DMI constants have a negative sign and therefore favor a counterclockwise rotational sense (Table II). The interlayer DMI, on the other hand, has a positive sign. This means that between the layers a clockwise rotation is preferred. These three interactions can be approximated by the an effective DMI favoring a counter clockwise rotational sense, i.e., $D_{\text{eff}} < 0$. Such a reduction of the effective DMI due to the interlayer DMI can also be seen in Fig. 10. The purple area representing the interlayer DMI reduces the total DMI contribution (black) compared to the sum of the intralayer DMI contributions (green). The $Rh/Fe_{fcc}/Co/Ir$ multilayer shows a similar qualitative behavior. Upon changing the stacking order of the Fe layer to hcp, we observe that the intralayer DMI constants exhibit opposite signs. However, D_{eff} is still small and negative.

It is striking that the DMI prefers the opposite rotational sense in these three magnetic bilayer systems with respect to the Rh/Co/Ir based multilayer. We recover the same rotational sense if we consider Co/Fe bilayer systems with an Fe/Ir interface (last two lines of Table II). There is a large positive contribution to the effective DMI constants from both the Fe/Ir interface and the interlayer DMI. The large effect of the interlayer DMI is also apparent from the energy dispersion due to SOC [cf. Fig. 10(d)].

5. Magnetocrystalline anisotropy energy

A second effect, which originates from SOC, is the magnetocrystalline anisotropy energy (MAE) defined as the total energy difference for a magnetization pointing along the in-plane vs the out-of-plane direction with respect to the magnetic layers. The MAE is given for the considered multilayers in Table III. A negative MAE represents an easy axis pointing in-plane with respect to the layers and a positive sign an out-of-plane easy axis. For the Co/Fe-bilayer based multilayers the MAE is given for a local fcc and hcp stacking of the Fe layer.

When comparing the Rh(2)/Co and Rh/Co/Ir multilayers, one can see that the easy axis turns from an out-of-plane direction with respect to the magnetic layers to an in-plane direction. For the Rh/Fe/Co/Ir, Rh(2)/Co/Fe/Ir(2), and Rh(2)/Co/Fe/Ir(3) multilayers the MAE decreases for the local hcp stacking of the Fe layer as well as for fcc stacking, i.e., an increasing Ir layer thickness weakens the out-of-plane easy axis. The MAE for hcp stacking of the Fe layer is also reduced with respect to the value for fcc stacking for all of these three multilayers. For the $Rh(2)/Co/Fe_{hcp}/Ir(3)$ multilayer this even leads to an easy in-plane magnetization direction.

TABLE III. Magnetocrystalline anisotropy energy (MAE) for different multilayer systems. A positive (negative) value denotes an out-of-plane (in-plane) easy magnetization axis with respect to the layers. All values are given in meV per magnetic atom. For systems containing Fe a local fcc and hcp stacking of the Fe layer is considered.

	fcc	hcp		
Rh/Co/Fe/Ir	−0.52	−1.16	Rh(2)/Co	0.1
Rh/Fe/Co/Ir	0.68	0.25	Rh/Co/Ir	−0.37
Rh(2)/Co/Fe/Ir(2)	0.57	0.13	Rh/Co(2)/Ir	2.51
Rh(2)/Co/Fe/Ir(3)	0.52	−0.39		

The Rh/Co(2)/Ir multilayer has a strong perpendicular magnetocrystalline anisotropy, when compared to Rh/Co/Fe/Ir. The Co layer seems to favor an out-of-plane orientation, which leads to a competition between the Co layer and the Ir layers. In the comparison to the Rh/Fe/Co/Ir multilayer one can see that the interface has an effect as well. When Co has no interface to Ir the magnetization favors an alignment in-plane with respect to the magnetic layers. Our calculations show that the magnetorystalline anisotropy energy and the easy axis depend quite sensitively on the stacking sequence, order, and number of 4*d* and 5*d* transition-metal layers in these multilayers built from a repetition of sandwich structures of only a few layers. However, a systematic study and analysis of the MAE upon increasing the number of Rh and Ir spacer layers is outside of the scope of our paper.

V. DISCUSSION

Within this paper, we have identified how the properties of multilayers consisting of Co, Fe, Rh, and Ir such as their chemical composition, stacking order, and sequence can influence the magnetic interactions due to hybridization at the interfaces leading to a large exchange frustration and significant DMI. The goal of our study was to find multilayer systems suitable for the stabilization of complex topological spin structures such as magnetic skyrmions. We can distinguish the investigated multilayers by the type of magnetic layers and can draw the following conclusions.

Single Co layer. In multilayers with a single magnetic Co layer such as Rh/Co/Ir significant exchange frustration occurs. The interplay between the resulting flat energy dispersion of spin spirals with moderate DMI and magnetocrystalline anisotropy energy still favors the ferromagnetic state. However, as pointed out in Sec. IV, we expect localized topological spin structures to occur as metastable states similar to the observations in ultrathin film systems [9].

Co/Co bilayer. In multilayers with two Co layers sandwiched in between Rh and Ir, both intra- and interlayer exchange interactions favor a ferromagnetic alignment of Co magnetic moments. The DMI in these systems is not strong enough (cf. Table I) to cant the magnetic moments out of their collinear order. Hence, in the presence of the magnetocrys-

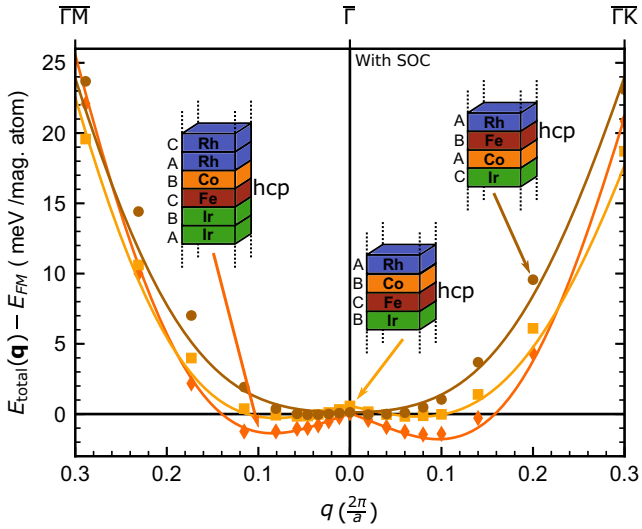

FIG. 11. Energy dispersions for cycloidal spin spirals including spin-orbit coupling, i.e., $E(\mathbf{q}) + \Delta E_{\mathrm{DMI}}(\mathbf{q}) + K/2$, for several Co/Fe based multilayers (see sketches) along the high symmetry direction $\overline{\mathrm{M}} - \overline{\Gamma} - \overline{\mathrm{K}}$. The total energies include the contributions from the exchange interaction $E(\mathbf{q})$, the DMI $\Delta E_{\mathrm{DMI}}(\mathbf{q})$, as well as the shift $K/2$, with respect to the FM state ($\mathbf{q} = 0$) due to the magnetocrystalline anisotropy energy. The symbols represent the data obtained by DFT. The solid lines show the fit to the spin model including exchange interaction and DMI.

talline anisotropy, we expect large ferromagnetic domains to form, which are separated by chiral domain walls.

Co/Fe *bilayer.* The most complex magnetic interactions occur in multilayers in which a Co/Fe bilayer is stacked between Rh and Ir layers. In such systems, the intralayer exchange interactions favor a ferromagnetic alignment of moments in the Co layer, while a spin spiral state is preferred in the Fe layer. The competition between these interactions in combination with ferromagnetic Co-Fe coupling leads to a strong exchange frustration. Depending on the particular stacking order and sequence, e.g., of the Fe layer, a spin spiral energy minimum or a ferromagnetic ground state occurs (see below). The DMI is enhanced in multilayers with an Fe/Ir interface. Because of the strong ferromagnetic coupling between the two magnetic layers for all considered systems we expect that emergent skyrmions behave simultaneously in the two layers as previously studied in other bilayer systems by atomistic spin simulations [53].

In order to obtain the energetically lowest magnetic state we show in Fig. 11 the total energy dispersions of spin spirals including SOC for three selected Co/Fe-bilayer based multilayers, which are most promising with respect to the occurrence of topological spin structures.

For the Rh/$\mathrm{Fe_{hcp}}$/Co/Ir multilayer the FM state ($\overline{\Gamma}$ point) is the magnetic ground state. Due to the interplay of frustrated exchange interactions and weak DMI (cf. Tables I and II) the energy dispersion rises only very slowly around the $\overline{\Gamma}$ point. The dispersion is very similar to that found for the ultrathin film system Rh/Co/Ir(111) and the Rh/Co/Ir multilayer (cf. Fig. 4). Since the easy magnetization axis is perpendicular to the magnetic layers (cf. Table III), we expect that this system might exhibit zero-field magnetic skyrmions as in Rh/Co/Ir(111) [9].

Upon changing the stacking order of the Co/Fe bilayer such that the Co layer is adjacent to the Rh layer and the Fe layer is adjacent to the Ir layer, resulting in the Rh/Co/$\mathrm{Fe_{hcp}}$/Ir multilayer, the strength of the DMI increases significantly (cf. Fig. 9 and Table II). This leads to a shallow energy minimum for a spin spiral state at $q \approx 0.06 \times \frac{2\pi}{a}$ in the total energy dispersion (Fig. 11). Therefore, a spin spiral state will occur in zero magnetic field as in the ultrathin film system Pd/Fe/Ir(111) [7,50]. However, since the magnetocrystalline anisotropy energy is quite large and prefers a magnetization within the plane of the atomic layers (cf. Table III), skyrmions will not appear in a magnetic field perpendicular to the magnetic layers. However, it is possible that bimerons [54], which can be viewed as in-plane analogues to skyrmions are stabilized due to the large exchange frustration.

The competition between exchange frustration and DMI depends on multilayer structure as can be seen from the calculation for a multilayer built from a repetition of Rh(2)/Co/$\mathrm{Fe_{hcp}}$/Ir(2) (Fig. 11). In this case, the energy minimum of the spin spiral ground state becomes a little deeper than in the previous case due a further increase of the DMI (see Table II). Since the easy magnetization axis is out-of-plane, we expect the emergence of skyrmions in an external magnetic field. The field strength for the transition to the skyrmion phase can be estimated to be on the order of 1 T since the energy minimum is about 1.5 meV/atom and the total magnetic moment of the Co/Fe bilayer is about 4 μ_{B}.

VI. CONCLUSIONS

In conclusion, we have demonstrated that the favorable magnetic properties of the ultrathin film system Rh/Co/Ir(111), i.e., frustrated exchange interactions and significant DMI, can be transferred to transition-metal multilayers with a similar stacking sequence. This may allow the realization of magnetic multilayers with zero-field skyrmions due exchange frustration observed in Rh/Co/Ir(111) [9]. In particular, a multilayer with a single atomic Co layer sandwiched between Ir and Rh layers shows the required strong exchange frustration and a similar magnitude of the DMI as in Rh/Co/Ir(111).

Since it is desirable to increase the number of magnetic layers in multilayers in order to allow their growth on larger scales we have studied ways to go beyond single magnetic layers. It turned out that the naive approach to use two Co layers sandwiched between Ir and Rh layers fails as the exchange interaction becomes strongly ferromagnetic while the DMI is reduced. However, we show that a sufficient exchange frustration can be obtained in multilayers based on Co/Fe bilayers. The interfaces to the magnetic layer of the isoelectronic materials Rh and Ir as well as the spacer thickness have minor influence on the exchange frustration. A local hcp stacking of the Fe layer leads to an even higher frustration. The DMI depends mostly on the interfaces between spacer and magnetic layer. A spacer thickness of a few layers of each material is beneficial because it makes the DMI more robust. The magnetocrystalline anisotropy energy in these Co/Fe bilayer based multilayers is not very robust and the

easy magnetization direction depends on the interfaces and local stacking sequence.

The magnetic ground state of the studied Co/Fe based multilayers is either ferromagnetic or exhibits a shallow spin spiral energy minimum. Multilayers with an easy in-plane direction might exhibit magnetic bimerons. It will be interesting to perform atomistic spin simulations based on the DFT parameters of all magnetic interactions provided in our paper.

ACKNOWLEDGMENTS

We gratefully acknowledge financial support from the Deutsche Forschungsgemeinschaft (DFG, German Research Foundation) through SPP2137 "Skyrmionics" (Project No. 462602351) and computing time provided by the North-German Supercomputing Alliance (HLRN).

APPENDIX A: Co/Rh(n) MULTILAYERS

We have also calculated the energy dispersion of spin spirals for multilayers with a single Co layer and a different number n of Rh spacer layers ranging from one to five (Fig. 12). These symmetric multilayers are denoted as Co/Rh(n). Due to the symmetry of the multilayers, the DMI is zero. Rh is isoelectronic to Ir and therefore these systems are expected to have similar properties as the Rh/Co/Ir multilayers discussed in the main text. For comparison we have performed a calculation for the corresponding ultrathin film system Rh/Co/Rh(111) [45].

The energy dispersion of the Co/Rh(n) multilayers look similar to that of the film system Rh/Co/Rh(111) [Fig. 12(a)]. However, the energy difference between the FM ($\overline{\Gamma}$ point) and the row-wise AFM state ($\overline{\mathrm{M}}$ point) is lower for the multilayers, which indicates a weaker nearest-neighbor FM exchange constant. The exchange frustration, which can be estimated from the region around the $\overline{\Gamma}$ point [see inset in Fig. 12(a)], varies a little for the multilayer systems with different number of Rh spacer layers. For the systems with $n = 2$ and 5 the rise of the energy dispersion close to $\overline{\Gamma}$ is similar to that of Rh/Co/Rh(111), which indicates that the exchange frustration is comparable. For the other multilayers, $E(\mathbf{q})$ rises more quickly with increasing spin spiral vector $|\mathbf{q}|$ and the exchange frustrations is smaller. Therefore, the thickness of the spacer layer can have an influence on the exchange frustration of the system.

The variation of the Co magnetic moments [Fig. 12(b)] for different systems is relatively small and does not have an effect on the exchange frustration. The variation of the moments with $|\mathbf{q}|$ is similar to that observed in the Rh/Co/Ir multilayers. Its effect on the exchange interaction is investigated in Appendix B. A significant magnetic moment is induced in the Rh layer adjacent to Co [Fig. 12(c)]. For the system Co/Rh(1) the magnetic moment is around twice as large as for the systems with more spacer layers since the Rh layer is directly adjacent to two Co layers.

For multilayer systems with only one magnetic Co layer, we find that an exchange frustration similar to that of the corresponding ultrathin film system is obtained for both Rh/Co/Ir and Co/Rh(n) multilayers.

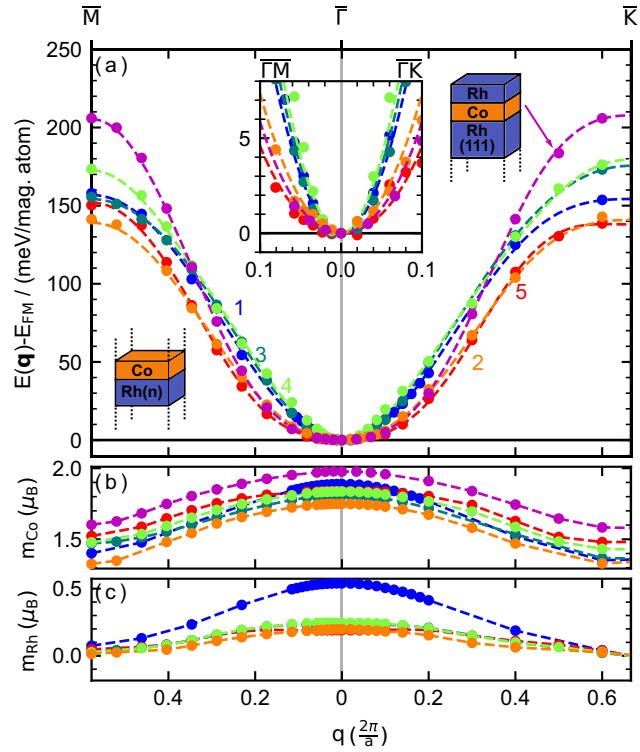

FIG. 12. (a) Energy dispersion $E(\mathbf{q})$ of spin spirals in the scalar-relativistic approximation, i.e., neglecting SOC, along the high-symmetry direction $\overline{\mathrm{M}} - \overline{\Gamma} - \overline{\mathrm{K}}$ for the multilayers Co/Rh(n) with n Rh spacer layers ($n = 1$ to 5) and the corresponding ultrathin film system Rh/Co/Rh(111). Symbols show the DFT data and lines the fit to the Heisenberg model. Energies are given with respect to the FM state ($\overline{\Gamma}$ point). The inset shows a zoom at the region around the $\overline{\Gamma}$ point. [(b),(c)] Magnetic moments of the Co layer and of the adjacent Rh layer. Symbols denote DFT data and dashed lines are a guide for the eye. The data for Rh/Co/Rh(111) were taken from Ref. [45].

APPENDIX B: CONICAL VS FLAT SPIN SPIRALS

In the atomistic spin model [Eq. (1)] it is assumed, that the magnitude of the magnetic moment at each atom site is constant. However, in the investigated transition-metal systems the magnetic moments of the 3d atoms change for spin spirals as a function of the wave vector $\mathbf{q}$ (cf. Fig. 12). This effect is smaller for Fe with its larger magnetic moment and a little more pronounced for Co. To estimate the effect of this change in magnetic moments on the exchange constants we have calculated the energy dispersion of conical spin spirals for the multilayer system Co/Rh(2). The normalized magnetic moment $\mathbf{m}_i$ at position $\mathbf{R}_i$ is given for a spin spiral vector $\mathbf{q}$ by

$$\mathbf{m}_i = \begin{pmatrix} \cos(\mathbf{q}\mathbf{R}_i)\sin(\vartheta) \\ \sin(\mathbf{q}\mathbf{R}_i)\sin(\vartheta) \\ \cos(\vartheta) \end{pmatrix}, \tag{B1}$$

where ϑ is the opening angle, which is 90° for flat spin spirals considered in the main text. For a smaller value of ϑ the tilting angle between neighboring spins is smaller for the same $\mathbf{q}$. Therefore, the deviation from a ferromagnetic alignment of all moments is smaller for varying $\mathbf{q}$ and thus the

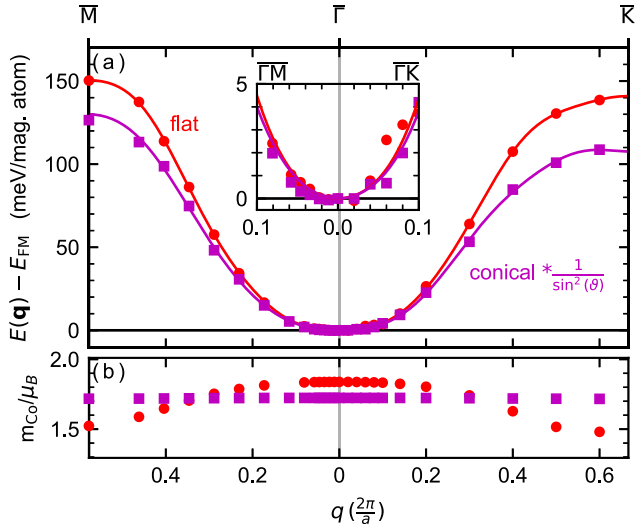

FIG. 13. (a) Energy dispersions $E(\mathbf{q})$ and (b) magnetic moments of Co for flat and conical spin spirals for the Co/Rh(2) multilayer. The opening angle for the conical spin spirals is $\vartheta = 10°$ and for the flat spin spirals it is $\vartheta = 90°$. The energy dispersion for the conical spin spirals have been scales with a factor $\sin^{-2}(\vartheta)$. The inset in (a) shows a zoom of the region around the $\overline{\Gamma}$ point.

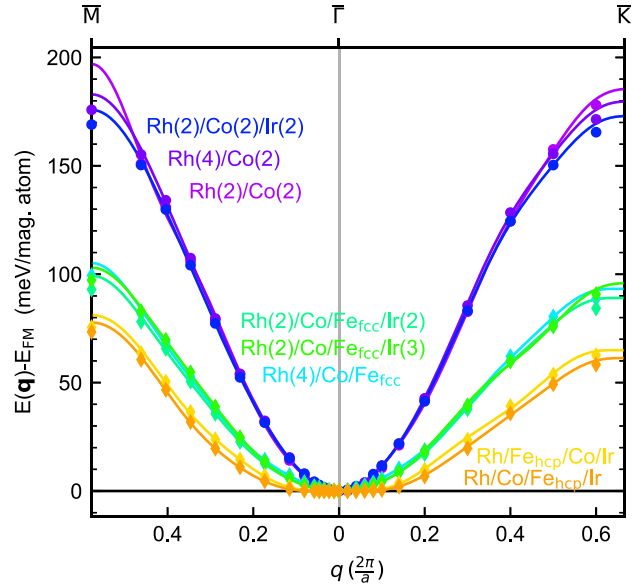

FIG. 14. Energy dispersions $E(\mathbf{q})$ for spin spirals calculated along the high-symmetry direction $\overline{\mathrm{M}} - \overline{\Gamma} - \overline{\mathrm{K}}$ in the scalar relativistic approximation, i.e., neglecting SOC; for multilayers from Co/Co and Co/Fe bilayers with different numbers of Rh and Ir spacer layers and local stacking environment of the Fe layer as indicated in the figure. The symbols denote DFT total energies and the lines represent the fit to the Heisenberg model.

change in the magnetic moments is smaller. The energy of a conical spin spiral with angle ϑ is expected to be $E_{\mathrm{conical}}(\mathbf{q}) = \sin^2(\vartheta) E_{\mathrm{flat}}(\mathbf{q})$ with respect to the FM state within the Heisenberg model of pairwise exchange. A disadvantage of the small tilting angle with respect to calculations is that the total energy differences becomes smaller such that the cut-off parameters have to be increased accordingly. For the calculations of the conical spin spirals a grid of $(64 \times 64 \times 23)$ **k** points and a cut-off parameter for the basis functions of $k_{\mathrm{max}} = 4.1$ a.u.$^{-1}$ were used.

In Fig. 13(a) the energy dispersions are displayed for the Co/Rh(2) multilayer for a flat spin spiral ($\vartheta = 90°$) and a conical spin spiral with $\vartheta = 10°$. The energy differences for the conical spin spiral have been scaled with a factor of $\sin^{-2}(\vartheta)$ in order to compare them with those of the flat spin spiral. The magnetic moments of the Co layer [Fig. 13(b)] are nearly constant for the conical spin spiral while they vary considerably with **q** in the case of the flat spin spiral. The energies around the $\overline{\mathrm{M}}$ and $\overline{\mathrm{K}}$ point differ by around 25 meV between both types of spin spirals. Thus there is a contribution of the varying magnetic moment, which is mapped onto the atomistic spin model if the energy dispersion of flat spirals is used. However, especially around the $\overline{\Gamma}$ point [inset of Fig. 13(a)] the dispersions of both spin spirals match very well. This region is of special interest for our work, as the ground state for all investigated systems is located in the vicinity of the $\overline{\Gamma}$ point. We conclude that flat spin spirals can give us a good insight into the magnetic interactions of the investigated systems and the energy landscape in the vicinity of the ground state.

From the atomistic spin model, Eq. (1), it follows that the energy due to Heisenberg exchange and DMI both scale with the same factor $\sin^2\vartheta$ for conical spin spirals. Therefore, conical and flat spin spirals will lead to the same ground state within the Heisenberg model including DMI. However, higher-order interactions could favour conical spin spirals over flat spin spirals as shown for the Mn double layer on W(110) in Ref. [55]. The very similar energy dispersion around the $\overline{\Gamma}$ point found in our calculations for multilayers (Fig. 13) indicates, that higher-order interactions have a negligible contribution in the systems investigated within this paper.

APPENDIX C: CATEGORIES OF Co/Co AND Co/Fe MULTILAYERS

In Sec. IV B we have categorized the investigated multilayer systems into three groups: the Co/Co bilayer, the Co/Fe bilayer with local fcc stacking of the Fe layer, and the Co/Fe-bilayer with a local hcp stacking of the Fe layer. For each of these groups one system is represented in Fig. 5 of the main text. In Fig. 14 we show the energy dispersions for more multilayer systems. There are basically three types of energy dispersions from which we have obtained the categories. For the group of Co/Co-bilayers we find the multilayers Rh(2)/Co(2), Rh(4)/Co(2) and Rh(2)/Co(2)/Ir(2). The systems Rh(2)/Co/Fe$_{\mathrm{fcc}}$/Ir(2), Rh(2)/Co/Fe$_{\mathrm{fcc}}$/Ir(3) and Rh(4)/Co/Fe$_{\mathrm{fcc}}$ belong to the Co/Fe-bilayer group with a local fcc stacking around the Fe layer. Finally, the systems Rh/Fe$_{\mathrm{hcp}}$/Co/Ir and Rh/Co/Fe$_{\mathrm{hcp}}$/Ir represent the group of Co/Fe-bilayers with a local hcp stacking around the Fe layer. It can be seen that all these systems show the same properties as described in the main text (Sec. IV B) according to their group.

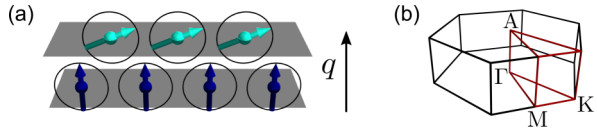

FIG. 15. (a) Flat cycloidal spin spin spirals with a propagation direction **q** perpendicular to the magnetic layers, i.e., along ΓA in the three-dimensional Brillouin zone (3D-BZ). (b) Sketch of the 3D-BZ in which the required high symmetry points are marked.

APPENDIX D: INTERLAYER EXCHANGE BETWEEN MAGNETIC LAYERS

In the main text we focused on the inter- and intralayer exchange interactions within a magnetic bilayer. In addition, there are magnetic interactions between those magnetic bilayers or between monolayers via the nonmagnetic Rh and Ir spacer layers. In this case it is also possible for the considered multilayers that the positions of magnetic atoms in interacting layers only differ in the vertical (z) coordinate. For spin spirals with **q** vectors taken from the 2D BZ such magnetic atoms always have the same spin direction and the interactions between them cannot be determined. Therefore, we have to use a spin spiral vector **q** from the 3D BZ (Fig. 15).

In principle, the interlayer interactions between bilayers can be resolved in shells as described for interactions within the bilayers in the main text. As the distance between bilayers, which are separated by a spacer of two or more layers, is much larger than the distance of direct adjacent magnetic layers in the same bilayer, the interlayer interactions between bilayers are much smaller than those within a bilayer. Therefore, we only calculate an effective interlayer interaction between magnetic layers separated by a spacer. This is achieved by calculating the energy dispersion for spin spirals between the high symmetry points Γ and A from the 3D BZ (Fig. 15). The spin structure, which corresponds to the A point, is the synthetic antiferromagnetic (SAF) state.

In Fig. 16 we display the energy differences between the FM and the SAF state $\Delta E_{\mathrm{FM-SAF}}$ for some of the multilayer systems considered in our study. Only one of the magnetic moments in the unit cell was set by the spin spiral vector **q** along $\overline{\Gamma} - \overline{A}$. All other magnetic moments were relaxed in direction as in Ref. [12] in order to obtain the structure with the minimal energy. We find that magnetic moments from the same magnetic layer always align ferromagnetically. For both magnetic configurations, the FM and the SAF state, all moments align parallel or antiparallel to each other and form a collinear spin structure.

We distinguish between different types of multilayers. The yellow marker in Fig. 16 denotes systems with only a single atomic layer in the magnetic layer. The marker connected by the blue dashed line represent the interlayer exchange energies of the hcp stacked Co/Rh(n) multilayer systems with $n = 1$ to 5. The marker connected with the red dash dotted line display the energy for the fcc stacked Rh/Co(n) systems. Whereas for all other calculations the primitive unit cell has been used, supercells were used for the interlayer exchange interactions of Co/Rh(n) with $n = 1$ to 5 to create an hcp or fcc stacking. Tests have shown that the stacking sequence has a minor influence on the intralayer exchange interaction within the magnetic layer in these systems.

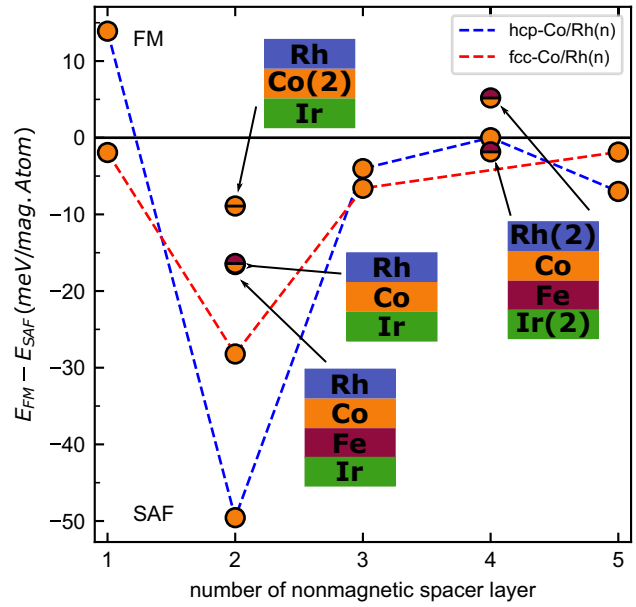

FIG. 16. Interlayer exchange interaction between the magnetic layers in a multilayer. The energy difference between the ferromagnetic and the synthetic antiferromagnetic (SAF) state are shown. A positive (negative) value indicates a FM (SAF) ground state. The blue (red) dashed line connects the energies for the systems Rh(n)/Co with $n = 1$ to 5 for hcp (fcc) stacking of the Co layer. The energies for the other systems are marked with icons, which represent the atomic layers of the unit cell of the particular multilayer system.

The energy difference $\Delta E_{\mathrm{FM-SAF}}$ varies in sign for the $\mathrm{Co_{hcp}}$/Rh(n) multilayers. For $n = 1, 4$ a FM alignment is favored, while for $n = 1$, 3, or 5 the SAF state is energetically preferred. The system with two Rh spacer layers has a very high interlayer coupling strength of about 50 meV. In comparison, the intralayer energy difference for $\mathrm{Co_{fcc}}$/Rh(2) between the row-wise AFM and the FM state is about 150 meV (cf. Fig. 12) and thus only three times larger. For $n = 2, 5$ the energies are shown as well for an fcc stacking, which exhibit smaller interlayer exchange strength than the corresponding multilayers in hcp stacking.

The three systems Rh/Co(2)/Ir, Rh/Co/Ir, and Rh/Co/Fe/Ir all possess a Rh/Ir spacer, which is two atomic layers thick. For these systems $\Delta E_{\mathrm{FM-SAF}} < 0$ (Fig. 16), i.e., the SAF state is favored, just as the Co/Rh(2) systems, which also exhibit two spacer layers. The systems Rh/Co/Fe/Ir and Rh/Co(2)/Ir can also be directly compared since they are constructed in the same unit cell of four atomic layers and the only difference is that one Co layer has been replaced by an Fe layer. As seen in Fig. 16, the multilayer with the Co bilayer has the smallest interlayer exchange energy $\Delta E_{\mathrm{FM-SAF}}$. This is consistent with a RKKY-like behavior since the Fe layer has a higher exchange splitting leading to larger reflection coefficients. When comparing the fcc stacked Co/Rh(2) with the fcc stacked Rh/Co/Ir one can see that the spacer layer has an influence on the strength of the interlayer exchange coupling, but the sign remains unchanged. The interlayer exchange of Rh/Co/Ir and Rh/Co/Fe/Ir is nearly identical.

For multilayers with four atomic spacer layers, the interlayer exchange energy is very small and similar for the

systems with a Co/Fe bilayer and a Co monolayer (Fig. 16). For the multilayer with a Co/Fe bilayer we have considered on one hand a perfect fcc stacking of all layers and on the other hand a stacking sequence of ABCACB for Rh(2)/Co/Fe_{hcp}/Ir(2) in which the Fe layer exhibits a local hcp environment. This change leads of the local stacking sequence from fcc to hcp leads to the opposite sign of the interlayer exchange interaction.

APPENDIX E: SHELL RESOLVED DMI PARAMETER FOR Rh/Co/Ir(111) AND Rh/Co/Ir

In Table IV the shell resolved DMI constants are given for the ultrathin film system Rh/Co/Ir(111) and the Rh/Co/Ir based multilayer as obtained by the fit shown in Fig. 4(b). As both systems possess only a single magnetic monolayer, no interlayer interactions occur.

TABLE IV. Shell resolved DMI constants for the ultrathin film system Rh/Co/Ir(111) and the multilayer system Rh/Co/Ir. The values were obtained by the fit shown in Fig. 4(b). Only interactions within the magnetic monolayer are considered. All values are given in meV per magnetic atom.

System	D_1	D_2	D_3	D_4	D_5	D_6	D_7
Rh/Co/Ir(111)	0.29	0.11	0.29	−0.03	0.02	−0.04	0.09
Rh/Co/Ir	−0.14	0.00	0.25	−0.03	0.04	0.03	0.00

[1] A. Bocdanov and A. Hubert, The properties of isolated magnetic vortices, Phys. Status Solidi B **186**, 527 (1994).

[2] N. Nagaosa and Y. Tokura, Topological properties and dynamics of magnetic skyrmions, Nat. Nanotechnol. **8**, 899 (2013).

[3] A. Fert, N. Reyren, and V. Cros, Magnetic skyrmions: Advances in physics and potential applications, Nat. Rev. Mater. **2**, 17031 (2017).

[4] C. Back, V. Cros, H. Ebert, K. Everschor-Sitte, A. Fert, M. Garst, T. Ma, S. Mankovsky, T. L. Monchesky, M. Mostovoy *et al.*, The 2020 skyrmionics roadmap, J. Phys. D: Appl. Phys. **53**, 363001 (2020).

[5] A. Fert, V. Cros, and J. Sampaio, Skyrmions on the track, Nat. Nanotechnol. **8**, 152 (2013).

[6] K. M. Song, J.-S. Jeong, B. Pan, X. Zhang, J. Xia, S. Cha, T.-E. Park, K. Kim, S. Finizio, J. Raabe *et al.*, Skyrmion-based artificial synapses for neuromorphic computing, Nat. Electron. **3**, 148 (2020).

[7] N. Romming, C. Hanneken, M. Menzel, J. E. Bickel, B. Wolter, K. von Bergmann, A. Kubetzka, and R. Wiesendanger, Writing and deleting single magnetic skyrmions, Science **341**, 636 (2013).

[8] N. Romming, A. Kubetzka, C. Hanneken, K. von Bergmann, and R. Wiesendanger, Field-Dependent Size and Shape of Single Magnetic Skyrmions, Phys. Rev. Lett. **114**, 177203 (2015).

[9] S. Meyer, M. Perini, S. von Malottki, A. Kubetzka, R. Wiesendanger, K. von Bergmann, and S. Heinze, Isolated zero field sub-10 nm skyrmions in ultrathin Co films, Nat. Commun. **10**, 3823 (2019).

[10] B. Dupé, G. Bihlmayer, M. Böttcher, S. Blügel, and S. Heinze, Engineering skyrmions in transition-metal multilayers for spintronics, Nat. Commun. **7**, 11779 (2016).

[11] A. Soumyanarayanan, M. Raju, A. L. G. Oyarce, A. K. C. Tan, M.-Y. Im, A. P. Petrović, P. Ho, K. H. Khoo, M. Tran, C. K. Gan *et al.*, Tunable room-temperature magnetic skyrmions in Ir/Fe/Co/Pt multilayers, Nat. Mater. **16**, 898 (2017).

[12] H. Jia, B. Zimmermann, and S. Blügel, First-principles investigation of chiral magnetic properties in multilayers: Rh/Co/Pt and Pd/Co/Pt, Phys. Rev. B **98**, 144427 (2018).

[13] H. Jia, B. Zimmermann, M. Hoffmann, M. Sallermann, G. Bihlmayer, and S. Blügel, Material systems for FM-/AFM-coupled skyrmions in Co/Pt-based multilayers, Phys. Rev. Mater. **4**, 094407 (2020).

[14] J. Wang, M. Strungaru, S. Ruta, A. Meo, Y. Zhou, A. Deák, L. Szunyogh, P.-I. Gavriloaea, R. Moreno, O. Chubykalo-Fesenko, J. Wu, Y. Xu, R. F. L. Evans, and R. W. Chantrell, Spontaneous creation and annihilation dynamics of magnetic skyrmions at elevated temperature, Phys. Rev. B **104**, 054420 (2021).

[15] E. Simon and L. Szunyogh, Spin-spiral formalism based on the multiple-scattering Green's function technique with applications to ultrathin magnetic films and multilayers, Phys. Rev. B **100**, 134428 (2019).

[16] C. Moreau-Luchaire, C. Moutafis, N. Reyren, J. Sampaio, C. A. F. Vaz, N. Van Horne, K. Bouzehouane, K. Garcia, C. Deranlot, P. Warnicke *et al.*, Additive interfacial chiral interaction in multilayers for stabilization of small individual skyrmions at room temperature, Nat. Nanotechnol. **11**, 444 (2016).

[17] S. Woo, K. Litzius, B. Krüger, M.-Y. Im, L. Caretta, K. Richter, M. Mann, A. Krone, R. M. Reeve, M. Weigand *et al.*, Observation of room-temperature magnetic skyrmions and their current-driven dynamics in ultrathin metallic ferromagnets, Nat. Mater. **15**, 501 (2016).

[18] O. Boulle, J. Vogel, H. Yang, S. Pizzini, D. de Souza Chaves, A. Locatelli, T. O. Menteş, A. Sala, L. D. Buda-Prejbeanu, O. Klein *et al.*, Room-temperature chiral magnetic skyrmions in ultrathin magnetic nanostructures, Nat. Nanotechnol. **11**, 449 (2016).

[19] L. Caretta, M. Mann, F. Büttner, K. Ueda, B. Pfau, C. M. Günther, P. Hessing, A. Churikova, C. Klose, M. Schneider *et al.*, Fast current-driven domain walls and small skyrmions in a compensated ferrimagnet, Nat. Nanotechnol. **13**, 1154 (2018).

[20] W. Legrand, D. Maccariello, F. Ajejas, S. Collin, A. Vecchiola, K. Bouzehouane, N. Reyren, V. Cros, and A. Fert, Room-temperature stabilization of antiferromagnetic skyrmions in synthetic antiferromagnets, Nat. Mater. **19**, 34 (2020).

[21] J. Jena, B. Göbel, T. Ma, V. Kumar, R. Saha, I. Mertig, C. Felser, and S. S. P. Parkin, Elliptical Bloch skyrmion chiral twins in an antiskyrmion system, Nat. Commun. **11**, 1115 (2020).

[22] L. Peng, R. Takagi, W. Koshibae, K. Shibata, K. Nakajima, T. hisa Arima, N. Nagaosa, S. Seki, X. Yu, and Y. Tokura, Controlled transformation of skyrmions and antiskyrmions in a non-centrosymmetric magnet, Nat. Nanotechnol. **15**, 181 (2020).

[23] F. Zheng, N. Kiselev, L. Yang, V. M. Kuchkin, F. N. Rybakov, S. Blügel, and R. E. Dunin-Borkowski, Skyrmion–antiskyrmion

pair creation and annihilation in a cubic chiral magnet, Nat. Phys. **18**, 863 (2022).
[24] A. O. Leonov and M. Mostovoy, Multiply periodic states and isolated skyrmions in an anisotropic frustrated magnet, Nat. Commun. **6**, 8275 (2015).
[25] S.-Z. Lin and S. Hayami, Ginzburg-Landau theory for skyrmions in inversion-symmetric magnets with competing interactions, Phys. Rev. B **93**, 064430 (2016).
[26] M. Goerzen, S. von Malottki, S. Meyer, P. F. Bessarab, and S. Heinze, Lifetime of coexisting sub-10 nm zero-field skyrmions and antiskyrmions, arXiv:2305.13018.
[27] Y. Zhang, C. Xu, P. Chen, Y. Nahas, S. Prokhorenko, and L. Bellaiche, Emergence of skyrmionium in a two-dimensional $CrGe(Se, Te)_3$ Janus monolayer, Phys. Rev. B **102**, 241107(R) (2020).
[28] D. Li, S. Haldar, and S. Heinze, Strain-driven zero-field near-10 nm skyrmions in two-dimensional van der Waals heterostructures, Nano Lett. **22**, 7706 (2022).
[29] H. Yang, J. Liang, and Q. Cui, First-principles calculations for Dzyaloshinskii–Moriya interaction, Nat. Rev. Phys. **5**, 43 (2023).
[30] P. Li, D. Yu, J. Liang, Y. Ga, and H. Yang, Topological spin textures in 1T-phase Janus magnets: Interplay between Dzyaloshinskii-Moriya interaction, magnetic frustration, and isotropic higher-order interactions, Phys. Rev. B **107**, 054408 (2023).
[31] See www.flapw.de.
[32] P. Kurz, F. Förster, L. Nordström, G. Bihlmayer, and S. Blügel, *Ab initio* treatment of noncollinear magnets with the full-potential linearized augmented plane wave method, Phys. Rev. B **69**, 024415 (2004).
[33] M. Heide, G. Bihlmayer, and S. Blügel, Describing Dzyaloshinskii-Moriya spirals from first principles, Phys. B: Condens. Matter **404**, 2678 (2009).
[34] C. Herring, in *Magnetism,* edited by G. Rado and H. Suhl (Academic Press, New York, 1966).
[35] L. M. Sandratskii, Energy band structure calculations for crystals with spiral magnetic structure, Phys. Status Solidi B **136**, 167 (1986).
[36] Note that SOC in first-order perturbation gives reliable results for the strength of the DMI as shown in Refs. [56,57].
[37] B. Zimmermann, M. Heide, G. Bihlmayer, and S. Blügel, First-principles analysis of a homochiral cycloidal magnetic structure in a monolayer Cr on W(110), Phys. Rev. B **90**, 115427 (2014).
[38] P. M. Levy and A. Fert, Anisotropy induced by nonmagnetic impurities in CuMn spin-glass alloys, Phys. Rev. B **23**, 4667 (1981).
[39] D.-S. Han, K. Lee, J.-P. Hanke, Y. Mokrousov, K.-W. Kim, W. Yoo, Y. L. W. van Hees, T.-W. Kim, R. Lavrijsen, C.-Y. You, H. J. M. Swagten, M.-H. Jung, and M. Kläui, Long-range chiral exchange interaction in synthetic antiferromagnets, Nat. Mater. **18**, 703 (2019).
[40] A. Fernández-Pacheco, E. Vedmedenko, F. Ummelen, R. Mansell, D. Petit, and R. P. Cowburn, Symmetry-breaking interlayer Dzyaloshinskii–Moriya interactions in synthetic antiferromagnets, Nat. Mater. **18**, 679 (2019).
[41] B. Van Waeyenberge, Bridging the gap, Nat. Mater. **18**, 657 (2019).
[42] E. Y. Vedmedenko, P. Riego, J. A. Arregi, and A. Berger, Interlayer Dzyaloshinskii-Moriya Interactions, Phys. Rev. Lett. **122**, 257202 (2019).
[43] C. Li, A. J. Freeman, H. J. F. Jansen and C. L. Fu, Magnetic anisotropy in low-dimensional ferromagnetic systems: Fe monolayers on Ag(001), Au(001), and Pd(001) substrates, Phys. Rev. B **42**, 5433 (1990).
[44] M. Bode, M. Heide, K. von Bergmann, P. Ferriani, S. Heinze, G. Bihlmayer, A. Kubetzka, O. Pietzsch, S. Blügel, and R. Wiesendanger, Chiral magnetic order at surfaces driven by inversion asymmetry, Nature (London) **447**, 190 (2007).
[45] S. Meyer, Complex spin structures in frustrated ultrathin films, Ph.D. thesis, Christian-Albrechts-Universität zu Kiel, 2020.
[46] J. P. Perdew, K. Burke, and M. Ernzerhof, Generalized Gradient Approximation Made Simple, Phys. Rev. Lett. **77**, 3865 (1996).
[47] S. H. Vosko, L. Wilk, and M. Nusair, Accurate spin-dependent electron liquid correlation energies for local spin density calculations: A critical analysis, Can. J. Phys. **58**, 1200 (1980).
[48] K. von Bergmann, S. Heinze, M. Bode, E. Y. Vedmedenko, G. Bihlmayer, S. Blügel, and R. Wiesendanger, Observation of a Complex Nanoscale Magnetic Structure in a Hexagonal Fe Monolayer, Phys. Rev. Lett. **96**, 167203 (2006).
[49] S. Heinze, K. von Bergmann, M. Menzel, J. Brede, A. Kubetzka, R. Wiesendanger, G. Bihlmayer, and S. Blügel, Spontaneous atomic-scale magnetic skyrmion lattice in two dimensions, Nat. Phys. **7**, 713 (2011).
[50] B. Dupé, M. Hoffmann, C. Paillard, and S. Heinze, Tailoring magnetic skyrmions in ultra-thin transition metal films, Nat. Commun. **5**, 4030 (2014).
[51] N. Romming, H. Pralow, A. Kubetzka, M. Hoffmann, S. von Malottki, S. Meyer, B. Dupé, R. Wiesendanger, K. von Bergmann, and S. Heinze, Competition of Dzyaloshinskii-Moriya and Higher-Order Exchange Interactions in Rh/Fe Atomic Bilayers on Ir(111), Phys. Rev. Lett. **120**, 207201 (2018).
[52] H. Yang, A. Thiaville, S. Rohart, A. Fert, and M. Chshiev, Anatomy of Dzyaloshinskii-Moriya Interaction at Co/Pt Interfaces, Phys. Rev. Lett. **115**, 267210 (2015).
[53] H. Schrautzer, S. von Malottki, P. F. Bessarab, and S. Heinze, Effects of interlayer exchange on collapse mechanisms and stability of magnetic skyrmions, Phys. Rev. B **105**, 014414 (2022).
[54] B. Göbel, A. Mook, J. Henk, I. Mertig, and O. A. Tretiakov, Magnetic bimerons as skyrmion analogues in in-plane magnets, Phys. Rev. B **99**, 060407(R) (2019).
[55] Y. Yoshida, S. Schröder, P. Ferriani, D. Serrate, A. Kubetzka, K. von Bergmann, S. Heinze, and R. Wiesendanger, Conical Spin-Spiral State in an Ultrathin Film Driven by Higher-Order Spin Interactions, Phys. Rev. Lett. **108**, 087205 (2012).
[56] S. Meyer, B. Dupé, P. Ferriani, and S. Heinze, Dzyaloshinskii-Moriya interaction at an antiferromagnetic interface: First-principles study of Fe/Ir bilayers on Rh(001), Phys. Rev. B **96**, 094408 (2017).
[57] B. Zimmermann, G. Bihlmayer, M. Böttcher, M. Bouhassoune, S. Lounis, J. Sinova, S. Heinze, S. Blügel, and B. Dupé, Comparison of first-principles methods to extract magnetic parameters in ultrathin films: Co/Pt(111), Phys. Rev. B **99**, 214426 (2019).